Biogeosystem Technique

Issued since 2014.

E-ISSN 2413-7316
2025. 12(2). Issued 2 times a year

Journal is indexed by: **Cross Ref (USA), Electronic scientific library (Russia), MIAR (Spain), Open Academic Journals Index (USA), CiteFactor – Directory of International Reseach Journals (Canada).**

All manuscripts are peer reviewed by experts in the respective field. Authors of the manuscripts bear responsibility for their content, credibility and reliability.

Editorial board doesn't expect the manuscripts' authors to always agree with its opinion.

Postal Address: 13906, Polarstone Ct., Houston, TX, 77044

Website: https://bgt.cherkasgu.press
E-mail: kalinitch@mail.ru

Founder and Editor: Cherkas Global University

Release date 25.12.25
Format 21 × 29,7/4.

Headset Georgia.

Order B-28.

Biogeosystem Technique

2025

Is. 2

CONTENTS

Articles

Published in the USA
Biogeosystem Technique
Issued since 2014.
E-ISSN: 2413-7316
2025. 12(2): 63-70

DOI: 10.13187/bgt.2025.2.63
https://bgt.cherkasgu.press

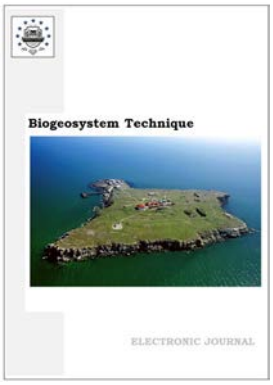

Articles

Forecasting the Spatiotemporal Dynamics of Trace-Element Concentrations in Soil Based on Multi-Year Monitoring

Armen Kirakosyan [a], Zaven Khanamiryan [a], Patrik Yesayan [a], Mushegh Aslikyan [b], Ara Galstyan [b], Astghik Sukiasyan [a, *]

[a] National Polytechnic University of Armenia, Yerevan, Armenia
[b] RA NAS "National Bureau of Expertises" SNPO, Armenia

Paper Review Summary:
Received: 2025, November 2
Received in revised form: 2025, November 24
Acceptance: 2025, November 30

Abstract

Mathematical forecasting methods were developed to evaluate the spatiotemporal dynamics of trace elements, including Fe, Zn, Cu, Mn, Cr, and V, in soils at the study sites. To detect trends and generate predictions, various models were employed, including linear and smoothing techniques. The trace-element composition in the studied soils shows moderate variability, mostly smooth and gradual, indicating the influence of long-term geochemical processes. Regional differences also emerged, highlighting the unequal impact of natural conditions and human activities on the trace-element background. These characteristics are crucial diagnostic tools for analyzing forecast results.

Keyword: trace metals, machine learning, spatiotemporal dynamics, linear regression, LOESS regression.

1. Introduction

Protecting the environment from pollution is critical to ensuring public safety and sustainable development. Natural environmental changes, alternating with anthropogenic impacts, alter natural geochemical cycles. A combination of the climatic factors, territory's lithological and geochemical features, soil formation conditions, and the intensity of economic activity determines the formation of spatial anomalies and temporal trends in chemical element content, especially heavy metals (HMs) (Sukiasyan et al., 2025). The situation is complicated by the fact that in the natural biogeochemical processes the HMs can accumulate and migrate within the soil, creating a long-term environmental hazard (Gall et al., 2015). Chemicals contaminating soil with HMs, mainly due to erosion and organic matter loss, are the primary results of declining soil fertility (Smith et al., 2024). The dynamics of HMs accumulation and migration in soils are determined by multiple physical, chemical, biological, and climatic factors (Zaky, Elwa, 2020; Kicińska et al., 2022).

* Corresponding author
E-mail addresses: sukiasyan.astghik@gmail.com (A. Sukiasyan)

However, the key determinants are the area's natural features such as relief, water permeability, and soil horizon's structure (de Matos et al., 2001). It has been established that small particles of HMs are washed from the upper slopes, leading to the formation of accumulation zones in the lower parts of the terrain (Ding et al., 2017). It is clear that achieving the Sustainable Development Goals requires moving towards integrated monitoring systems that account not only for the total content of elements but also for their chemical distribution in the soil environment, mobility, and availability to living organisms (Tóth et al., 2016).

In recent years, ecological research has increasingly shifted from basic measurements of metal content to detailed evaluations of their environmental risks. The use of multivariate statistical methods, geoinformation technologies, and ecological risk indices enables researchers to identify sources, spatial distributions, and potential threats. This progression lays the groundwork for scientifically grounded pollution control and impact mitigation strategies (Gong et al., 2024).

Spatiotemporal changes in the chemical composition of soils are a key focus in environmental research, as soils act as accumulators and converters of elemental constituents, reflecting both natural and anthropogenic processes (Shi et al., 2023). The development of spatial anomalies and temporal trends in soil element content results from a combination of climate factors, lithological and geochemical terrains, soil formation conditions, and moderate economic activity (Zhuo et al., 2019). Analysing these changes helps evaluate the current condition of ecosystems and guides their future development. Among HMs, trace elements (TEs) are particularly prominent; they occur at much lower concentrations but play a crucial role in the functioning of biological and geochemical systems (Sukiasyan, Kirakosyan, 2024).

TEs are involved in oxidation-reduction processes. They regulate other chemical elements migration. TEs respond to environmental changes, and indicate the soils mineralogical features and the soils long-term chemical variations (Zhang et al., 2022; Xu et al., 2023; Islam et al., 2023). A typical feature of the content of TEs in the soil cover is its spatial and temporal variability (Wang et al., 2020; Taghizadeh-Mehrjardi et al., 2021). This is why modern research is increasingly aimed not only at describing soils' current conditions but also at creating predictive models for their spatiotemporal changes (Córdoba et al., 2025).

The aim of this study is to analyze the spatiotemporal dynamics of selected TEs in soil samples from different regions of Armenia, drawing on multi-year monitoring data, with a focus on predicting changes in their concentrations using mathematical models.

2. Materials and methods

The study is based on monitoring data on the content of TEs Fe, Zn) Cu, Mn, Cr and V) in the soils of the regions Gegharkunik (Gavar and Martuni sites) and Kotayk (Hrazdan sites) is situated in the eastern part of Armenia (Figure. 1). At least five soil samples from the same site at the control points, obtained using the envelope method to a depth of up to 20 cm, were mixed. The samples were subsequently placed in dark glass containers and transported at +4°C for 24 hours for instrumental measurements in the laboratory. Direct X-ray exposure was used for elemental analysis of all soil samples using a portable XRF analyser (Thermo Scientific™ Niton™) (Sukiasyan et al., 2022).

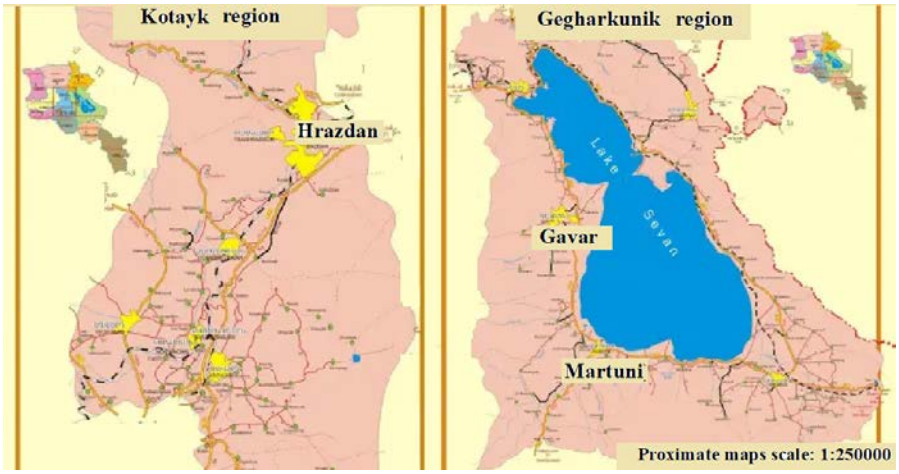

Fig. 1. Soil sampling region of Armenia

The initial time series spans from 2021 to 2023 and shows the average regional element concentrations. For analysis, averaged indicators across regions were utilised to focus on common spatiotemporal patterns. To create and forecast the temporal behaviour of TEs, various mathematical models were employed, including linear regression (LR), exponential smoothing (ETS), and locally estimated scatterplot smoothing (LOESS) regression (Hyndman, Koehler, 2002; Koyande, 2024). LOESS is a non-parametric regression method that performs local polynomial fits. It applies a low-degree polynomial to data subsets using weighted least squares, where the weights depend on the distance to the target point. This approach is particularly effective at identifying non-linear patterns, such as sudden rises or falls in metal levels. For each metal, a second-degree polynomial was fitted using LOESS, producing a locally adaptive model that predicts smooth, flexible future trends (Cleveland, Devlin, 1988).

The fitted polynomial takes the general form:

$$\hat{z}_{t+k} = \sum_{i=1}^{n} \omega_i(t+k) P_i(t+k) \quad (1)$$

where: $\hat{z}_{t+k}$ - is the future values of concentration in log-space at year x_{t+k}; $P_i(t+k)$ is a local polynomial (degree 2); $w_i(t+k)$ are weights based on proximity to t, controlled by a span parameter.

Coefficients of the fitted curve:

$$\hat{y}_t = a \cdot t^2 + b \cdot t + cy \quad (2)$$

where a, b, and c are coefficients determined through local fitting.

The final predicted concentration can be calculated by:

$$\hat{y}_{t+k} = \exp(\hat{z}_{t+k}) \quad (3)$$

Model parameters were estimated individually for each TE and site. A comparative analysis of these results helped evaluate the consistency of the forecasts and the robustness of the identified trends. Forecasts were made for 2024-2026 to analyse changes in soil TE composition.

Data processing and model development employed standard statistical methods. Results were interpreted considering established geochemical mechanisms that control the migration and accumulation of TEs in soils.

3. Results and discussion

The selection of Zn, Cu, Fe, Mn, Cr, and V for regional analysis is due to their physicochemical characteristics, marked by high chemical reactivity in soil and strong responsiveness to local geochemical conditions. Based on the concentration data, a forecast of the temporal behaviour of TEs was created using mathematical models, including LR, ETS, and LOESS (Tables 1-3).

Table 1. Parameters of the linear regression model for soil sampling sites

Trace Element / Parameters	Zn	Cu	Fe	Mn	Cr	V
Hrazdan sites						
Intercept $\beta 0$	-251.02	171.45	-342.42	-52.56	735.68	-557.29
Slope β_1	0.13	-0.08	0.17	0.03	-0.37	0.28
Gavar sites						
Intercept $\beta 0$	-46.17	-153.11	-165.31	-151.53	557.94	-453.42
Slope β_1	0.02	-0.07	0.09	0.08	-0.28	0.23
Martuni sites						
Intercept $\beta 0$	186.70	299.65	-141.66	126.75	-350.33	-380.33
Slope β_1	-0.09	-0.15	0.8	-0.06	0.18	0.19

Table 2. Parameters of the exponential smoothing model for soil sampling sites

Trace Element / Parameters	Zn	Cu	Fe	Mn	Cr	V
Hrazdan sites						
Level	4.56	4.41	10.23	6.72	4.45	4.72
Trend	0.13	-0.12	0.17	0.03	0.37	0.28
Damping	0.995	0.800	0.995	0.995	0.995	0.995
Initial Level	99.27	85.10	29633.10	849.07	97.73	124.87
Initial Trend	0.03	-16.53	-1772.30	-26.23	-3.03	-2.77
Gavar sites						
Level	4.50	4.41	10.48	6.66	4.62	4.78
Trend	0.04	-0.11	0.090	0.08	0.28	0.23
Damping	0.80	0.80	0.995	0.995	0.995	0.995
Initial Level	84.40	38515.00	819.65	113.30	113.50	130.55
Initial Trend	-13.27	-5694.33	-63.95	-5.80	-5.80	-4.38
Martuni sites						
Level	4.47	4.26	10.33	6.63	4.85	4.67
Trend	-0.09	-0.21	0.08	-0.06	0.17	0.19
Damping	0.995	0.800	0.995	0.995	0.995	0.995
Initial Level	71.80	31548.45	737.40	135.30	135.30	116.55
Initial Trend	-14.35	-700.75	4.10	-3.35	-3.35	-7.85

Table 3. Parameters of the locally weighted scatterplot smoothing model for soil sampling sites

Trace Element / Parameters	Zn	Cu	Fe	Mn	Cr	V
Hrazdan sites						
a	0.13	0.13	0.24	0.06	0.40	0.30
b	-509.92	-539.41	-954.84	-245.51	-1608.13	-1214.92
c	5.15e+05	5.45e+05	9.65e+05	2.48e+05	1.63e+06	1.23e+06

Gavar sites						
a	-0.11	0.10	0.247	0 . 16	0.33	0.26
b	430.53	-394.08	-988.66	-644.96	-1337.90	-1054.75
c	-4.35e+05	3.99e+05	1.01e+06	6.52e+05	1.35e+06	1.07e+06
Martuni sites						
a	-0.06	0.08	0.10	0.26	0.20	0.26
b	256.64	-310.73	-394.90	-1053.07	-811.55	-1052.18
c	-2.59e+05	3.14e+05	3.99e+05	-2.66e+05	8.20e+05	1.06e+06

Using the specified parameters, predicted changes in TE concentrations in soil samples across all research sites through 2026 were modelled using LR, ETS, and LOESS (Figure 2).

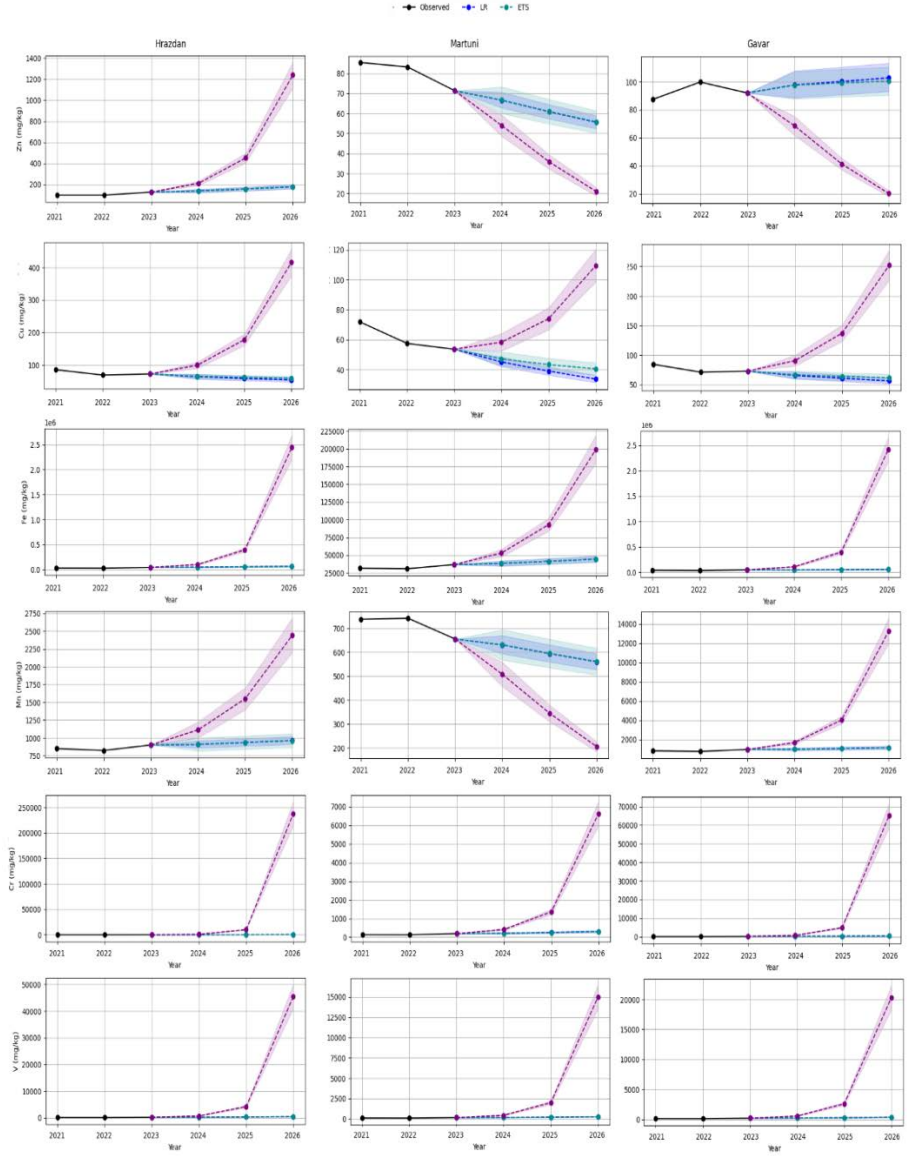

Fig. 2. Predicted trajectories of change in TE concentrations (Zn, Cu, Fe, Mn, Cr, and V) in the soils at the Hrazdan, Martuni, and Gavar sites up to 2026

For Zn, regional differences are particularly notable. At the Hrazdan sites, LR captures the ongoing directional trends over the forecast period, whereas ETS smooths fluctuations to produce a more stable trajectory. LOESS highlights local nonlinear patterns, influenced by regional factors. At Gavar and Martuni, forecast curves are more stable with minimal differences between LR and ETS, while LOESS shows slight deviations. Confidence intervals for Zn expand over time, especially for LR and LOESS, but remain within the observed range, supporting forecast interpretation. This pattern aligns with Zn's chemistry as a moderately mobile element influenced by pH and organic matter.

Cu concentration in all three regions is highly consistent across models. The predicted LR trajectories are smooth; ETS further diminishes fluctuations, and LOESS uncovers only minor nonlinear effects. Regional variations are moderate and do not cause significant differences in forecast estimates. Confidence intervals are relatively narrow and gradually widen without sudden jumps. This forecast stability is consistent with copper's chemical behaviour in soil, where it tends to bind strongly to organic matter and mineral components, restricting its movement and stabilising its temporal dynamics, even in the presence of anthropogenic activities.

Cu concentration in all three regions is highly consistent across models. The predicted LR trajectories are smooth; ETS further diminishes fluctuations, and LOESS uncovers only minor nonlinear effects. Regional variations are moderate and do not cause significant differences in forecast estimates. Confidence intervals are relatively narrow and gradually widen without sudden jumps. This forecast stability is consistent with copper's chemical behaviour in soil, where it tends to bind strongly to organic matter and mineral components, restricting its movement and stabilising its temporal dynamics, even in the presence of anthropogenic activities.

A notably different perspective emerges when examining Fe. Even after considering regional differences, all models show marked forecast volatility. LR predicts sharply rising trends in all regions, ETS enhances this trend, and LOESS highlights the nonlinear complexity of the time series. Confidence intervals widen quickly and considerably, especially in 2025-2026, signalling high uncertainty in future estimates. This model volatility underscores iron's fundamental role as a redox-sensitive element and a key geochemical regulator: transitions between Fe^{2+} and Fe^{3+} are linked to oxide phase formation, causing sudden and hard-to-predict shifts in concentrations.

Similar patterns have been observed for Mn. At the Hrazdan sites, the LR and ETS forecast curves show growth, while LOESS produces trajectories with sharp bends, highlighting the nonlinear nature of the dynamics. At the Gavar sites, the forecasts are somewhat smoother, but the overall trend of high variability remains. Confidence intervals quickly widen and become disproportionately large, signaling low forecast stability. This behaviour aligns with the chemical properties of Mn, which, like Fe, participates actively in redox reactions and can significantly change its soil speciation (Mn^{2+}/Mn^{4+}) with minor pH shifts.

Regarding Cr, regional analysis also fails to produce stable forecast estimates. In all regions, LR shows sharp upward trends, ETS amplifies the growth trend, and LOESS highlights the strong nonlinearity of the time series. Predicted values quickly surpass observed levels, and confidence intervals expand substantially. This indicates Cr's valence instability and significant differences in the mobility and toxicity of its various forms, meaning even minor environmental changes can cause disproportionate concentration shifts.

Finally, V behaves similarly to Cr and Mn. Overall, the LR and ETS projections show a clear upward trend across all sites, with LOESS capturing sharp local variations. Confidence intervals widen quickly and peak at the end of the forecast, suggesting vanadium's dynamics are highly unpredictable. This pattern is consistent with its chemistry, which features a complex valence system and high redox sensitivity.

4. Conclusion

A comparison of forecasting methods revealed notable differences. LR was sensitive to directional shifts and best captured overall trends in regions with stable dynamics. However, under high variability, it often overestimated predictions. ETS proved effective at smoothing short-term fluctuations and providing more stable forecasts for elements with moderate reactivity, such as Zn and Cu. Yet this method does not accurately model systems with strong redox-dependent dynamics.

Using LOESS allowed the detection of local nonlinear features in the time series that parametric models miss. This method was especially useful for analyzing spatial differences, but its predictive stability diminishes with shorter time series, restricting its effectiveness for long-term forecasts.

The results indicated that regional forecasting provides clear and consistent estimates for chemically stable and complexing elements like Zn and Cu. However, for redox-sensitive elements such as Fe, Mn, Cr, and V, significant uncertainty persists even when using a spatial approach. This highlights the inherent limitations of time-based models in accurately representing elements whose concentrations are more influenced by changes in soil physicochemical conditions than by temporal variations.

References

Cleveland, Devlin, 1988 – *Cleveland, W.S., Devlin, S.J.* (1989). Locally Weighted Regression: An Approach to Regression Analysis by Local Fitting. *Journal of the American Statistical Association*. 83(403): 596-610.

Córdoba et al., 2025 – *Córdoba, M.A., Hang, S.B., Bozzer, C., Alvarez, C., Faule, L., Kowaljow, E., Vaieretti, M.V., Bongiovanni, M.D., Balzarini, M.G.* (2025). Spatial Variability and Temporal Changes of Soil Properties Assessed by Machine Learning in Córdoba, Argentina. *Soil Systems*. 9(4): 109. DOI: https://doi.org/10.3390/soilsystems9040109

de Matos et al., 2001– *de Matos, A.T., Fontes, M.P., da Costa, L.M., Martinez, M.A.* (2001). Mobility of heavy metals as related to soil chemical and mineralogical characteristics of Brazilian soils. *Environmental Pollution*. 111(3): 429-435. DOI: 10.1016/s0269-7491(00)00088-9

Ding et al., 2017 – *Ding, Q., Cheng, G., Wang, Y., Zhuang, D.* (2017). Effects of natural factors on the spatial distribution of heavy metals in soils surrounding mining regions. *Science of The Total Environment*. 578: 577-585. DOI: 10.1016/j.scitotenv.2016.11.001

Gall et al., 2015 – *Gall, J.E., Boyd, R.S., Rajakaruna, N.* (2015). Transfer of heavy metals through terrestrial food webs: a review. *Environmental Monitoring and Assessment*. 187: 187-201. DOI: https://doi.org/10.1007/s10661-015-4436-3

Gong et al., 2024 – *Gong, J., Gao, J., Wu, H., Lin, L., Yang, J., Tang, S., Wang, Z., Duan, Z., Fu, Y., Cai, Y., Hu, S., Li, Y.* (2024). Heavy metal spatial distribution, source analysis, and ecological risks in the central hilly area of Hainan Island, China: results from a high-density soil survey. *Environmental geochemistry and health*. 46(6): 210. DOI: https://doi.org/10.1007/s10653-024-02031-1

Hyndman, Koehler, 2002 – *Hyndman, R.J., Koehler, A.B.* (2002). Forecasting with exponential smoothing: Some guidelines for model selection. *International Journal of Forecasting*. 22(4): 443-473.

Islam et al., 2023 – *Islam, M.R., Akash, S., Jony, M.H., Alam, M.N., Nowrin, F.T., Rahman, M.M., Rauf, A, Thiruvengadam, M.* (2023). Exploring the potential function of trace elements in human health: a therapeutic perspective. *Molecular and Cellular Biochemistry*. 478(10): 2141-2171. DOI: https://doi.org/10.1016/j.catena.2021.105766

Kicińska et al., 2022 – *Kicińska, A., Pomykała, R., Izquierdo-Diaz, M. (2022).* Changes in soil pH and mobility of heavy metals in contaminated soils. *European Journal of Soil Science*. 73(1): e13203. DOI: https://doi.org/10.1111/ejss.13203

Koyande, 2024 – *Koyande, T.* (2024). Assumption Checking of a Multiple Linear Regression Model. *International Journal of Research in Technology and Innovation*. 8(7): 322-325.

Shi et al., 2023 – *Shi, J., Zhao, D., Ren, F., Huang, L.* (2023). Spatiotemporal variation of soil heavy metals in China: The pollution status and risk assessment. *The Science of the total environment*. 871: 161768. DOI: https://doi.org/10.1016/j.scitotenv.2023.161768

Smith et al., 2024 – *Smith, P., Poch, R.M., Lobb, D.A., Bhattacharyya, R., Alloush, G., Eudoxie, G., Anjos, L.H., Castellano, M., Ndzana, G.M., Chenu, C., Naidu, R., Vijayanathan, J., Muscolo, A.M., Studdert, G., Eugenio, N.R., Calzolari, M.C., Amuri, N.A., Hallett, P.* (2024). Status of the World's Soils. *Annual Review of Environment and Resources*. 49: 73-104. DOI: doi.org/10.1146/annurev-environ-030323-075629

Sukiasyan, Kirakosyan, 2024 – *Sukiasyan, A.R., Kirakosyan, A.A.* (2024). Seasonal aspects of macro, trace, and ultra trace element changes in soils with different anthropogenic loads. *Sustainable Development of Mountain Territories*. 16: 789-802. DOI: https://doi.org/10.21177/1998-4502-2024-16-2-789-802

Sukiasyan et al., 2022 – *Sukiasyan, A., Simonyan, A., Kroyan, S., Hovhannisyan, A., Vardanyan, V., Okolelova, A., Kirakosyan, A.* (2022). Assessing the geo-environmental risks of

technogenic pollution of agricultural soils. *Biogeosystem Technique*. 9(2): 89-100. DOI: 10.13187/bgt.2022.2.89

Sukiasyan et al., 2025 – *Sukiasyan, A.R., Yesayan, P.A., Khanamiryan, Z.G., Kirakosyan, A.A.* (2025). Predicting concentration change of some TMs in soil–water ecosystem using machine learning. *Proceedings of the YSU C: Geological and Geographical Sciences.* 59(2). 266: 574-583. DOI: https://doi.org/10.46991/PYSUC.2025.59.2.574

Taghizadeh-Mehrjardi et al., 2021 – *Taghizadeh-Mehrjardi, R., Fathizad, H., Ali Hakimzadeh Ardakani, M., Sodaiezadeh, H., Kerry, R., Heung, B., Scholten, T.* (2021). Spatio-Temporal Analysis of Heavy Metals in Arid Soils at the Catchment Scale Using Digital Soil Assessment and a Random Forest Model. *Remote Sensing*. 13(9): 1698. DOI: https://doi.org/10.3390/rs13091698

Tóth et al., 2016 – *Tóth, G., Hermann, T., Da Silva, M.R., Montanarella, L.* (2016). Heavy metals in agricultural soils of the European Union with implications for food safety. *Environment International.* 88: 299-309. DOI: 10.1016/j.envint.2015.12.017

Wang et al., 2020 – *Wang, H., Yilihamu, Q., Yuan, M., Bai, H., Xu, H., Wu, J.* (2020). Prediction models of soil heavy metal(loid)s concentration for agricultural land in Dongli: A comparison of regression and random forest. *Ecological Indicators*. 119. DOI: https://doi.org/10.1016/j.ecolind.2020.106801

Xu et al., 2023 – *Xu, Y., Bi, R. Li, Y.* (2023). Effects of anthropogenic and natural environmental factors on the spatial distribution of trace elements in agricultural soils. *Ecotoxicology and Environmental Safety*. 249: 114436. DOI: https://doi.org/10.1016/j.ecoenv.2022.114436

Zaky, Elwa, 2020 – *Zaky, M.H., Elwa, A-S.M.* (2020). Heavy metals content relating to soil physical properties. *Egyptian Journal of Applied Science*. 35(5): 50-62.

Zhang et al., 2022 – *Zhang, T., Sun, F., Lei, Q., Jiang, Z., Luo, J., Lindsey, S., Xu, Y., Liu, H.* (2022). Quantification of soil element changes in long-term agriculture: A case study in Northeast China. *Catena*. 208: 105766. DOI: 10.1016/j.catena.2021.105766

Zhuo et al., 2019 – *Zhuo, Z., Xing, A., Li, Y., Huang, Y., Nie, C.* (2019). Spatio-Temporal Variability and the Factors Influencing Soil-Available Heavy Metal Micronutrients in Different Agricultural Sub-Catchments. *Sustainability*. 11(21): 5912. DOI: https://doi.org/10.3390/su11215912

Published in the USA
Biogeosystem Technique
Issued since 2014.
E-ISSN: 2413-7316
2025. 12(2): 71-78

DOI: 10.13187/bgt.2025.2.71
https://bgt.cherkasgu.press

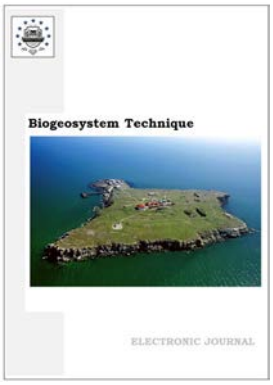

Invasive Plant Monitoring in Hard-To-Reach Areas Using Swarms of Agricultural Drones

Vasiliy Yu. Rud' [a, b, *], Denis A. Egorov [a], Rafek R. Abdullin [a], Nataliya V. Krupenina [a], Vladimir E. Marley [a], Ivan V. Rud [a], Maxim V. Dyuldin [c], Zhenyue Yuan [d], Van Yuikun [e], Artem A. Markaryan [f]

[a] Admiral Makarov State University of Maritime and Inland Shipping, Saint-Petersburg, Russian Federation
[b] Ioffe Physico-Technical Institute, Saint-Petersburg, Russian Federation
[c] Peter the Great St. Petersburg Polytechnic University, Saint-Petersburg, Russian Federation
[d] Shenyang Institute of Technology, Fushun, China
[e] Wenzhou University, Wenzhou, China
[f] Sechenov First Moscow State Medical University, Moscow, Russian Federation

Paper Review Summary:
Received: 2025, November 4
Received in revised form: 2025, November 24
Acceptance: 2025, November 30

Abstract

The article is devoted to the issues of organization of monitoring and control of invasive plants growing in hard-to-reach places using a swarm of drones and a drone port. Sosnovsky's hogweed has spread widely in Russia and is actively seizing new areas, creating infestation steps that are difficult to control using traditional methods. Monitoring and elimination of such foci by traditional manual methods is time-consuming, ineffective and unsafe.

A new technology that provides rapid monitoring of large areas and targeted chemical intervention only where necessary, reducing the risk of damage from invasions and the use of pesticides, is a technology based on the use of a drone swarm in conjunction with a drone port. It allows you to quickly explore large areas and get detailed images of growing vegetation from different angles. The resulting images can be recognized by means of artificial intelligence, analyzing the density of growth of invasive plants and their proximity to other crops.

The data collected by agrodrones can be conditionally divided into digital and graphical. When receiving digital data from a swarm of drones, the information on the drone port is cleaned of noise and checked for consistency to ensure the reliability of the data, which improves the efficiency of system maintenance. For graphic data, first of all, color correction is used, restoring color details and increasing clarity, while restoring the natural image distorted at the time of digitization and subsequent processing.

The key issue is the merging of the data collected by the agrodron swarm. Different specimens of agrodrons can receive different parameters and different images of the same habitat of invasive

* Corresponding author
E-mail addresses: ecobaltica@gmail.com (V.Yu. Rud)

plants, and these data need to be linked to each other, eliminating contradictions. After building a consistent model of the area, the growing plants are recognized using artificial intelligence.

The described technology allows automated analysis of the vegetation condition and provides conclusions and recommendations based on artificial intelligence.

Keywords: invasive plants, swarm of agricultural drones, data cleaning, data fusion.

1. Problem Statement of Monitoring

Weed infestation presents a pressing issue in agriculture, significantly reducing crop yields and, in certain cases, posing serious threats to ecosystems, agricultural productivity, and human health. In Russia, the spread of Heracleum sosnowskyi (Sosnowsky's hogweed) is particularly acute. This plant forms dense thickets up to 3 meters tall and secretes a toxic sap that causes severe phytophotodermatitis in humans. Ambrosia artemisiifolia (common ragweed) has become widespread in southern regions, triggering potent allergic reactions – its pollen being a notorious allergen – and diminishing field productivity (Müllerová, 2024) Solidago canadensis (Canada goldenrod) and related species aggressively displace native flora, establishing monocultures that degrade pollinator habitats and disrupt ecosystem services These and other invasive weeds continuously colonize new territories, creating invasion foci that are difficult to control using conventional methods.

Traditional manual approaches to monitoring and eradicating such infestations are labor-intensive, time-consuming, inefficient, and potentially hazardous. For example, ground-based surveys of hogweed-infested areas are impeded by the risk of chemical burns while locating ragweed across expansive fields demands substantial human resources. Moreover, blanket pesticide application over entire fields results in excessive chemical loading on the environment. Thus, novel technologies are required that enable rapid, large-scale monitoring and facilitate precise, localized interventions only where necessary – thereby mitigating ecological damage and minimizing chemical usage.

The advancement of unmanned aerial vehicles (UAVs), or agricultural drones, offers transformative potential in addressing this challenge. UAVs allow rapid coverage of extensive areas and provide high-resolution visual data through aerial imagery (Figure 1). They enable timely and comprehensive field inspections, facilitate the identification of weed clusters, reduce inspection time, and permit detailed, multi-angle examination of detected infestations (Monteiro, Santos, 2022). Artificial intelligence (AI) algorithms can then be applied to classify plant species visible in the captured images (Dutech, Scherrer, 2013).

Although the deployment of agricultural UAVs remains somewhat limited in Russia at present, the topic of agro-drones remains highly relevant – not only domestically but globally. Increasingly, "smart" technological solutions are emerging that reduce operational costs and optimize agro-industrial complex (AIC) workflows. Drones play a pivotal role in the digital transformation of the AIC. Consequently, UAV developers continue to introduce increasingly sophisticated and multifunctional models tailored to diverse agricultural tasks.

Fig. 1. Application of agricultural drones in farming

Of particular interest is the use of drone swarms – coordinated groups of UAVs operating in conjunction with a central droneport. While a single drone is constrained by flight range and endurance, a swarm can efficiently cover large areas and complete missions far more effectively. Cooperative control necessitates robust inter-drone communication and avoidance of task duplication. Modern algorithms enable real-time data exchange and collaborative coverage path planning, wherein each UAV autonomously computes its flight trajectory while accounting for the plans of others. Distributed coordination and information sharing maximize area coverage while minimizing energy consumption. A key challenge lies in the preliminary processing and cleaning of acquired data, as well as its fusion across multiple UAVs and the resolution of inconsistencies between overlapping observations.

2. Hardware Configuration for Monitoring

To perform monitoring tasks effectively, a drone must be equipped with the following instrumentation:

1. A high-resolution camera for capturing detailed imagery;
2. An ultrasonic sensor for obstacle detection and collision avoidance;
3. A Bluetooth module for short-range data transmission;
4. A GPS receiver for geotagging the location of each data capture;
5. An accelerometer for maintaining horizontal stabilization and minimizing deviations;
6. A barometric sensor (barometer) for altitude hold;
7. An autopilot system for autonomous waypoint navigation and return-to-home functionality.

The drone must incorporate obstacle-avoidance sensors capable of triggering evasive maneuvers upon detecting obstructions. Its internal control system should enable autonomous flight along pre-defined routes even in the event of communication loss with the ground control station.

The drone must be outfitted with a high-resolution camera, as it is required to approach a designated field segment, descend to a low altitude, and capture multiple high-quality images. Upon mission completion, the collected data must be transmitted to the droneport, where specialized software leveraging AI algorithms performs subsequent analysis and interpretation.

3. Data Cleaning

Data acquired by agricultural drones can be broadly categorized into two types: digital (numerical sensor readings) and graphical (imagery).

All transmitted and received signals inherently contain noise – defined as any undesirable signal component superimposed on the ideal signal. In digital wireless communication systems, the ideal signal resembles a trapezoidal pulse, which becomes distorted in the presence of noise (Figure 2; Li, 2009).

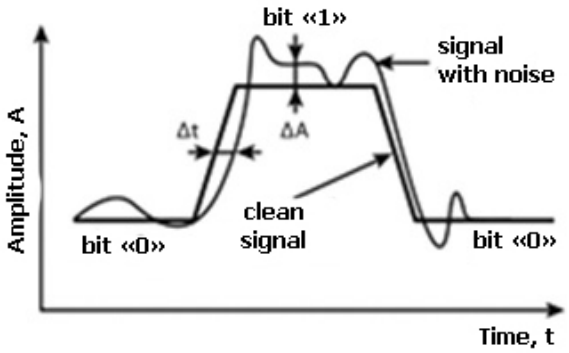

Fig. 2. Ideal vs. real signal waveforms

Deviations from the ideal can be observed in both time (temporal jitter) and amplitude (amplitude noise). In radio-frequency systems, signal amplitude corresponds to power; thus, amplitude deviation (dA) represents amplitude noise, while temporal deviation (dt) constitutes jitter.

Jitter-unwanted timing instability – manifests as fluctuations in the temporal positioning of signal transitions relative to their nominal values. It arises from synchronization instability and channel path variations. Jitter comprises two components: a purely random (stochastic) component and a quasi-deterministic, typically low-frequency component known as wander (Smagin, 2012).

The effects of jitter and amplitude noise on system performance are asymmetric. Amplitude noise acts as a continuous function, exerting a persistent influence on system characteristics. In contrast, jitter affects the system only during signal edge transitions.

Signal integrity is generally defined as any deviation from the ideal signal waveform. Thus, it encompasses both amplitude noise and jitter. However, certain integrity issues – such as undershoot, overshoot, and signal ringing – cannot be fully characterized solely by jitter and noise metrics (Figure 3).

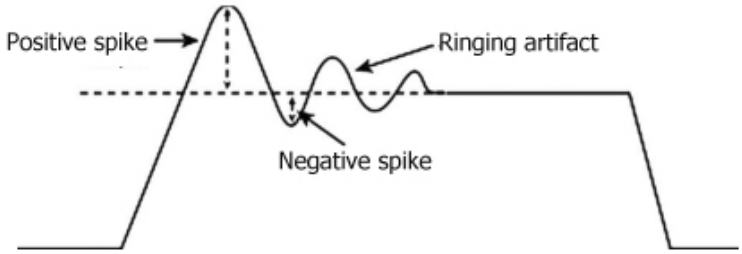

Fig. 3. Characteristics of signal integrity

The combined impact of jitter and amplitude noise is best evaluated from the perspective of the receiver in a communication system. The receiver samples the incoming pulse at time t using a voltage threshold v (Figure 4). In the ideal case, sampling occurs at the center of the input pulse. If the rising and falling edge times satisfy t_f < t_s and the signal voltage V₁ > v_s, the system correctly registers a logical “1” (Figure 4a).

In the presence of jitter and noise, signal edges shift along the time axis and voltage levels fluctuate along the amplitude axis. This may violate the conditions for correct bit detection, leading to bit errors (e.g., a logical “1” misinterpreted as “0”). Three failure modes may occur during “1” detection:

1. The rising edge crosses the threshold after the sampling instant (t_f > t_s);

2. The falling edge crosses before the sampling instant (t_f < t_s);

3. The signal voltage falls below the threshold (V₁ < v_s).

For logical “0” detection (Figure 4b), correct sampling requires t_r < t_s < t_f and V₀ < v_s. Violations mirror those for “1,” except that V₀ > v_s leads to error.

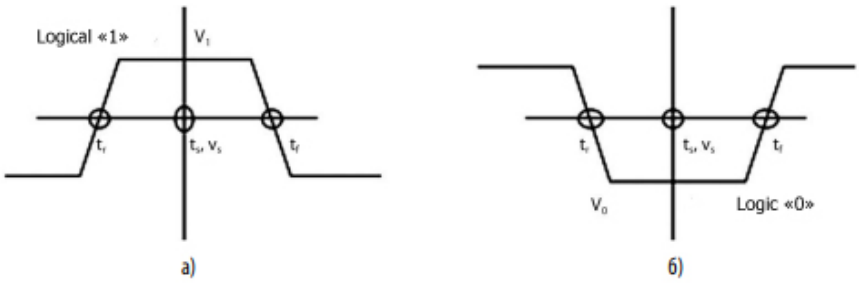

Fig. 4. Receiver-based sampling of input data

Given that digital systems transmit numerous bits over time, overall performance is commonly quantified by the Bit Error Rate (BER) – the ratio of erroneous bits (N_{err}) to total transmitted bits (N_{tot}). BER serves as a fundamental quality metric for communication systems. At multi-gigabit-per-second data rates, standards such as Fibre Channel, Gigabit Ethernet, SONET, and PCI Express typically require BER ≤ 10^{–12}, meaning

no more than one error per trillion bits. Higher BER degrades network efficiency and increases system latency. BER depends on data rate, jitter, and noise, and – being statistical – is often analyzed using Poisson statistics.

Jitter and noise originate from numerous physical and systemic sources, broadly classified as intrinsic and extrinsic. Intrinsic sources stem from the stochastic behavior of electrons and holes in semiconductor devices and represent fundamental physical limits that cannot be fully eliminated – though they may be minimized. Extrinsic sources arise from system design and configuration and are thus potentially correctable.

Intrinsic noise primarily results from thermal and shot noise in electronic and optoelectronic components, setting baseline constraints on system dynamic range. Noise is typically quantified in terms of voltage, current, or power – collectively referred to as "amplitude." When amplitude noise ΔA(t) is superimposed on a base signal A₀(t), the corresponding timing jitter can be approximated via linear small-signal perturbation theory:

$$
\Delta t \approx \frac{\Delta A(t)}{dA_0/dt}
$$

where dA₀/dt is the signal slew rate (Figure 5). Thus, for a given amplitude noise level, timing jitter decreases as the signal edge steepness increases – highlighting the benefit of minimizing rise/fall times to reduce jitter.

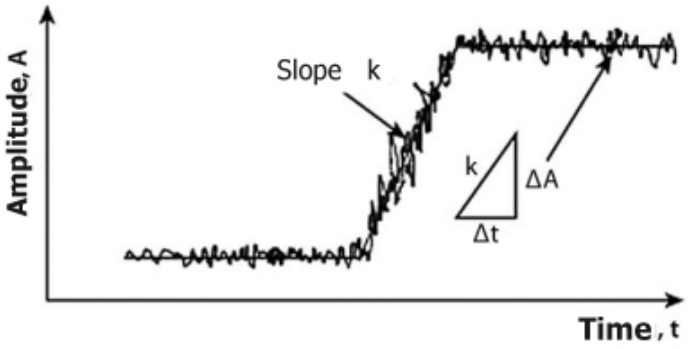

Fig. 5. Conversion of amplitude noise into timing jitter according to linear perturbation theory

Extrinsic noise and jitter arise from system-level imperfections and are amenable to mitigation. Common types include periodic modulation (phase, amplitude, or frequency), duty cycle distortion, inter-symbol interference, crosstalk, electromagnetic interference (EMI), and reflections due to impedance mismatches.

Digitally acquired sensor data undergoes preliminary filtering on board the drone or at the droneport processor to prevent heavily corrupted data from entering the operational database. Cleaned data is then accumulated in real time within a centralized data repository.

Effective noise filtering enhances measurement accuracy (Baklanov, 1998) and sensor reliability. Two primary noise types must be addressed: (1) stationary (additive white Gaussian noise) with relatively stable amplitude, and (2) impulsive noise caused by external disturbances.

For stationary noise, the moving average filter is well-suited: it maintains a buffer of recent measurements and shifts the observation window forward with each new sample. Although this method involves floating-point calculations that slightly slow processing, the overhead remains negligible compared to data transmission latency (FourWeekMBA, 2025).

Impulsive noise within individual measurements is best mitigated using a median filter (Smagin, 2012). Empirical studies show that combining median filtering with moving average yields robust results.

Of special interest is the filtering of the quasi-deterministic jitter component, which primarily reflects hardware-specific characteristics. To isolate this component, we propose the "Caterpillar" method – also known as Singular Spectrum Analysis (SSA). A key advantage of SSA is that it requires no prior model of the jitter process. SSA decomposes a time series into interpretable components (trend, periodicities, noise) by embedding the series into a trajectory matrix, performing singular value decomposition (SVD), and reconstructing selected components. This

approach outperforms conventional time-series methods in separating structured signal features from noise.

Following onboard preprocessing, cleaned data is transmitted via communication channels to the central droneport computer for advanced analysis.

Graphical data – i.e., aerial imagery – also requires cleaning. This includes correcting or removing corrupted information such as duplicates, missing values, incorrect formats, and outliers.

Color correction is an essential step in digital image processing. Manual white balance settings on cameras often introduce uncontrolled color inaccuracies. Although modern image editors provide powerful correction tools, manual intervention is impractical in high-throughput workflows. Fortunately, automated color correction solutions exist.

Image quality enhancement focuses on restoring natural color fidelity and improving sharpness – reversing distortions introduced during capture or digitization. Advanced algorithms automatically identify regions requiring adjustment (e.g., color balance, brightness, contrast) and apply localized corrections. These systems also address common artifacts such as moiré patterns and color casts.

Sophisticated color grading leverages blending algorithms and lookup tables (LUTs) to not only restore faded colors but also modify the original color palette as needed.

Professional tools such as iCorrect EditLab – a plugin for Adobe Photoshop and other leading graphic editors – offer fully automated color correction (SmartAgro, 2025). The software analyzes the entire image, identifies predefined color classes (e.g., sky blue, foliage green, human skin tones), and aligns corrections with the host application's color management settings.

iCorrect EditLab operates in four sequential stages:

1. Neutral tone balancing: Identifies mid-gray regions to eliminate color casts;
2. White/black point detection: Sets dynamic range endpoints;
3. Saturation, contrast, and brightness adjustment;
4. Natural color restoration: Recalibrates individual hues to reflect real-world appearance.

4. Data Fusion

A critical challenge lies in processing and fusing data collected by a swarm of UAVs. Different drones may capture varying measurements or images of the same field segment, necessitating reconciliation and conflict resolution.

First, high-accuracy monitoring requires integrating heterogeneous data sources: RGB imagery, multispectral data, LiDAR point clouds, and thermal imaging. Such data fusion significantly enhances weed detection accuracy. Studies confirm that combining spectral, textural, and thermal features yields superior classification performance compared to single-modality approaches (FourWeekMBA, 2025; Monteiro, Santos, 2022).

Second, even homogeneous data (e.g., visible-spectrum photographs from multiple drones) exhibit overlapping regions that must be seamlessly stitched. Generating consistent orthomosaics and vegetation maps from partially overlapping images is essential to avoid gaps or duplicate counting of the same plants.

5. Image Recognition via Artificial Intelligence

Object detection in drone-captured imagery is framed as a classification problem within an AI system. Solving it requires a pre-assembled image database of regional flora, partitioned into training and validation sets. A neural network is then trained on this dataset to classify plant species in new, incoming images.

Since ground-truth labels (correct species identifications) are available for training samples, this constitutes a supervised learning task. The goal is to assign each detected plant to its correct taxonomic class. Unrecognized species – those absent from the training set – may be flagged as "unknown." Accumulation of numerous such cases would necessitate model retraining with expanded data.

The machine learning (Malinowski et al., 2025) pipeline for plant classification is illustrated in (Figure 6).

By aggregating observations from the drone swarm and classifying detected vegetation, a detailed spatial map of invasive species distribution and density can be constructed. This enables targeted intervention strategies – ranging from precision herbicide application to localized mechanical removal – optimizing resource use and ecological impact.

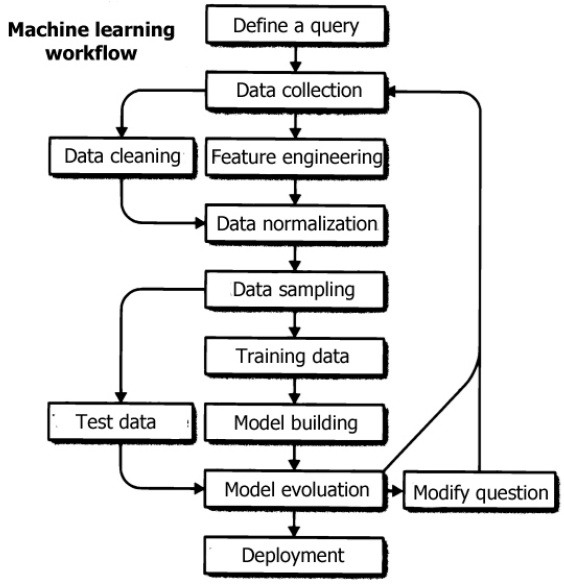

Fig. 6. Stages of the machine learning process

6. Advantages of Drone Swarm Monitoring

Compared to conventional field inspection methods, agricultural drone swarms offer the following advantages:

1. Rapid area coverage: Depending on model, a single drone can monitor 2–6 hectares in 10–20 minutes. Swarm deployment parallelizes this process, drastically reducing total inspection time.

2. Operation in complex terrain: High maneuverability and terrain-following sensors enable obstacle avoidance and effective monitoring on slopes, wetlands, and other inaccessible areas where tractors or personnel cannot operate.

3. Geospatial precision: GPS-enabled data ensures accurate mapping and repeatable monitoring.

4. All-weather and day/night operability: Equipped with appropriate sensors (e.g., thermal, NIR), drones function independently of lighting or meteorological conditions.

5. Cost efficiency: UAVs significantly reduce expenditures on ground machinery, fuel, and labor.

6. Multifunctionality: Modern drones support advanced features such as waypoint marking, mission pause/resume, multi-payload coordination, and centralized task management.

Agronomists traditionally face significant time and labor demands in routine field inspections. The integration of NDVI (Normalized Difference Vegetation Index) maps enables real-time vegetation monitoring, highlighting priority zones for ground verification.

NDVI quantifies vegetation presence and health by analyzing reflected light in visible and near-infrared (NIR) bands (Li, 2009). Chlorophyll-rich, healthy plants strongly absorb red light (used in photosynthesis) and reflect NIR due to intact cellular structure. Stressed or sparse vegetation exhibits the opposite pattern. Thus, NDVI serves as a proxy for crop vigor.

However, NDVI indicates that a problem exists – not why. Season-long NDVI trend analysis is essential for accurate diagnosis.

NDVI data is collected via satellites or UAVs equipped with NIR cameras, operating from orbital altitudes down to ~700 m. This enables high-resolution, actionable field maps.

The data acquisition workflow includes:

1. Equipment calibration for specific crops and conditions;

2. Placement of ground control points;

3. Aerial image capture;

4. Georeferencing of all field segments.

Post-processing yields detailed vegetation health maps, empowering agronomists to prioritize interventions and forecast yields.

Sentinel-2 satellite imagery provides NDVI at 10 m/pixel resolution, enabling fine-scale analysis – superior to other optical indices limited to 20 m/pixel. Nevertheless, NDVI has

limitations: its sensitivity declines at high canopy densities, and persistent cloud cover can degrade data quality, necessitating complementary radar or UAV-based sensing.

Moreover, NDVI performs poorly in fields with low vegetation cover or during early growth stages. In such cases, the MSAVI (Modified Soil-Adjusted Vegetation Index) offers a robust alternative. MSAVI accounts for soil background effects (color, moisture), making it particularly effective during early season monitoring when soil is still visible between sparse seedlings.

6. Conclusion

The deployment of agricultural drone swarms for monitoring crop fields substantially enhances agronomic efficiency. By automating visual inspection, enabling precise weed detection, and leveraging AI-driven analytics, this approach significantly boosts labor productivity in agriculture while supporting sustainable, data-driven decision-making.

References

Müllerová, 2024 – *Müllerová, J.* (2025). Heracleum mantegazzianum (giant hogweed). CABI Digital Library. DOI: https://doi.org/10.1079/cabicompendium.26911 (date of access: 21.03.2025).

Monteiro, Santos, 2022 – *Monteiro, A., Santos, S.* (2022). Sustainable Approach to Weed Management: The Role of Precision Weed Management. *Agronomy*. 12: 118-130.

FourWeekMBA, 2025 – Noise Filtering. FourWeekMBA. [Electronic resource]. URL: https://fourweekmba.com/noise-filtering/ (date of access: 16.10.2025).

Malinowski et al., 2025 – *Malinowski, R., Krupiński, M., Skórka, P., Mikołajczyk, L., Chuda, K., Lenda, M.* (2025). Harnessing remote sensing and machine learning techniques for detecting and monitoring the invasion of goldenrod invasive species. *Sci Rep*. 15: 32222. DOI: https://doi.org/10.1038/s41598-025-17440-0

Smagin, 2012 – *Smagin, S.A.* (2012). Application of the "Caterpillar" Method for Extracting the Quasi-Deterministic Jitter Component in Communication Channels. *Izvestiya VUZ. Povolzhskiy Region. Technical Sciences*. 1(21): 37-46.

Baklanov, 1998 – *Baklanov, I.G.* (1998). Measurement Technologies in Modern Telecommunications. Moscow: ECO-TRENDS.

Dutech, Scherrer, 2013 – *Dutech, A., Scherrer, B.* (2013). Partially Observable Markov Decision Processes. In *Markov Decision Processes in Artificial Intelligence*; Sigaud, O., Buffet, O., Eds.; John Wiley & Sons, Inc.: Hoboken, NJ, USA. Chapter 7. Pp. 185-228.

SmartAgro, 2025 – NDVI Imagery for Field Monitoring. SmartAgro. [Electronic resource]. URL: https://smartagro.ru/ndvi-snimki/ (date of access: 16.10.2025).

Li, 2009 – *Li, M.P.* (2009). Jitter, Noise, and Signal Integrity in High-Speed Communication Systems. *Electronic Components*. 10: 81-85. [Electronic resource]. URL: https://russianelectronics.ru/files/47193/EK10_81-85.pdf

Published in the USA
Biogeosystem Technique
Issued since 2014.
E-ISSN: 2413-7316
2025. 12(2): 79-84

DOI: 10.13187/bgt.2025.2.79
https://bgt.cherkasgu.press

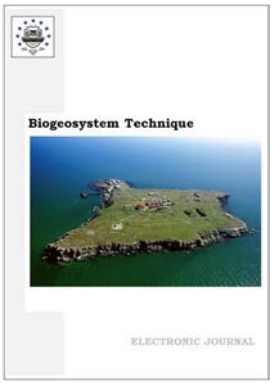

Monitoring Features of the Pipeline Systems Condition

Vasiliy Yu. Rud' [a, b, *], Denis A. Egorov [a], Nataliya V. Krupenina [a], Vladimir E. Marley [a], Ivan V. Rud [a], Eugeny O. Ol'khovik [a], Maxim V. Dyuldin [c], Rafek R. Abdullin [a], Zhenyue Yuan [d], Van Yuikun [e]

[a] Admiral Makarov State University of Maritime and Inland Shipping, Saint-Petersburg, Russian Federation
[b] Ioffe Physico-Technical Institute, Saint-Petersburg, Russian Federation
[c] Peter the Great St. Petersburg Polytechnic University, Saint-Petersburg, Russian Federation
[d] Shenyang Institute of Technology, Fushun, China
[e] Wenzhou University, Wenzhou, China

Paper Review Summary:
Received: 2025, November 4
Received in revised form: 2025, November 22
Acceptance: 2025, November 30

Abstract

The article is devoted to the consideration of topical issues of organizing continuous monitoring of the pipeline system for pumping extracted natural gas and oil in hard-to-reach places based on the use of a drone port and a swarm of drones. A large amount of natural resources is extracted in the coastal shelf of the northern seas, where the water surface is covered with ice most of the time, and monitoring of the pipeline system by means of the auxiliary fleet is possible only during a short period of navigation, therefore automation of the monitoring process will allow for year-round monitoring and timely identification of emerging problems for their prompt elimination.

Using a drone swarm with a droneport base station makes it possible to increase the efficiency of obtaining information by obtaining it more quickly from several alternative sources and then merging them. When information is received from the drone, the information is cleared of noise and checked for consistency to ensure a higher level of data reliability, which improves the efficiency of system maintenance. Data is cleared from noise by the drone port, while merging data from coherent sources and building a visual model of the pipeline system status is performed by a stationary computer after data is transmitted from the drone port via fiber-optic communication channels. The visual model, combined with parametric data obtained from sensors installed inside the pipeline, allows artificial intelligence systems to predict potential emergency conditions and plan routine repairs of the pipeline infrastructure until a real accident occurs with serious consequences. The introduction of an automated continuous monitoring system will allow the pipeline to be operated according to its actual technical condition, thereby reducing operating costs and ensuring the safety of its operation.

Keywords: monitoring, pipeline system, drone port, drone swarm.

* Corresponding author
E-mail addresses: ecobaltica@gmail.com (V.Yu. Rud)

1. Introduction

Energy constitutes one of the foundational sectors of the economy and plays a critical role in sustaining modern society (Atdaeva et al., 2024). It encompasses not only resource generation challenges but also issues related to distribution and consumption.

Currently, oil and coal extracted from the Earth's subsurface represent the predominant share of global energy resources. As is well known, these reserves within the Earth's crust are finite; consequently, humanity actively seeks equivalent substitutes.

Replacing coal and oil with natural gas substantially reduces harmful atmospheric emissions, thereby contributing to the preservation of the Earth's ozone layer and improving the operational efficiency of thermal power plants.

Significant volumes of natural resources are extracted from the continental shelves of northern seas, raising the acute challenge of transporting these commodities to the mainland. While maritime shipping is widely employed for this purpose, vessel-based delivery of oil and natural gas represents a highly costly undertaking – particularly in northern seas, where such operations become infeasible during winter months due to ice cover. Pipeline transportation presents a viable alternative, offering greater economic efficiency and reduced operational complexity.

Pipeline operation for oil and gas transportation necessitates continuous condition monitoring through readings from embedded sensors, supplemented by periodic external inspections. For submerged pipeline sections, such activities can only be conducted using auxiliary vessels and exclusively during ice-free periods – a condition that, in northern seas, occurs for only a brief annual window. Relying on auxiliary fleets for pipeline monitoring constitutes a costly seasonal operation feasible solely in the absence of ice cover. Given that pipeline failures may occur at any time of year, the implementation of alternative monitoring methodologies becomes imperative.

2. Materials and methods

Pipeline inspection monitoring represents a comprehensive suite of non-destructive testing (NDT) and diagnostic procedures designed to identify defects (corrosion, cracks, deformations), assess residual wall thickness, verify weld integrity, and evaluate insulation quality. These procedures employ techniques including ultrasonic testing, radiography, liquid penetrant and magnetic particle inspection, as well as visual examination – often integrated within automated systems for continuous monitoring and residual service life assessment.

The principal objectives of pipeline monitoring include:

1. Defect detection: Identification of corrosion, erosion, cracks, dents, and pitting.
2. Geometric control: Measurement of wall thickness and deviations from design geometry.
3. Weld assessment: Verification of joint quality.
4. Component diagnostics: Examination of valves, flanges, supports, and hangers.
5. Insulation evaluation: Assessment of anticorrosive coating and thermal insulation integrity.

3. Discussion and results

The overarching purpose of monitoring is to ensure the safety and reliability of pipeline infrastructure, prevent accidents and gas leaks, facilitate maintenance planning, and extend the operational lifespan of pipeline assets. Pipeline failure in aggressive marine environments poses severe ecological consequences.

For monitoring pipelines in inaccessible locations, automated inspection using unmanned aerial vehicles (UAVs), commonly termed drones, offers a practical solution. However, a single drone proves inefficient for rapid assessment of extensive pipeline segments; consequently, drone swarms coordinated by a specialized hub – the drone port – are typically deployed.

A drone port constitutes an advanced unmanned technology complex designed for automated drone deployment, recovery, and maintenance to support pipeline section monitoring. The primary limitation of autonomous drones remains restricted operational duration due to battery capacity constraints. Even with contemporary lithium-ion batteries, modern quadcopters rarely sustain flight beyond 30 minutes. Drone ports address this limitation by providing infrastructure for drone recovery, recharging, and preparation for subsequent inspection missions. This infrastructure enables the establishment of continuous automated monitoring networks capable of rapid response to unforeseen operational incidents.

Such drone ports have already been implemented for monitoring terrestrial pipeline segments in remote terrain. For instance, the HIVE drone port (Figure 1) can replace a drone's battery in under three minutes. Additionally, it transmits acquired data to a central server and simultaneously charges up to four battery pairs. Through the HIVE system, drones maintain near-continuous operational readiness. In 2022, HIVE underwent field testing at facilities operated by SIBUR Holding. Previously, Moscow's municipal search and rescue service tested the drone port over water bodies. Deployment of HIVE commenced in Innopolis, Tatarstan, in 2020 (Zhang et al., 2021).

Fig. 1. HIVE drone port, Russia

Integrated with the drone port, a swarm of observation drones equipped with sensor arrays performs dual functions: acquiring data from pipeline-embedded sensors and conducting autonomous surveillance of pipeline infrastructure integrity and ambient environmental parameters – including air temperature and chemical composition – to detect leaks and support ecological monitoring. Such drones may be outfitted with high-resolution cameras, thermal imagers, gas analyzers, and supplementary sensors (Figures 2, 3; Faniadis, Amanatiadis, 2020).

For marine pipeline segment inspection, deployment of a seabed platform connected to onshore energy and data resources via subsea cable is proposed. This platform would facilitate recharging of marine monitoring drone swarms and aggregate transmitted data for preprocessing, fusion, and relay to coastal monitoring stations. Development of such seabed platforms is currently underway.

Fig. 2. DJI Matrice 300 RTK drone with Zenmuse H20T payload and U10 gas analyzer

Underwater drones have gained utility in pipeline monitoring owing to their capacity to operate within inaccessible and hazardous submerged environments. These vehicles can descend to considerable depths, withstand saline water exposure, and capture high-fidelity imagery using integrated cameras – including 4K resolution systems. Control methodologies encompass tethered teleoperation, radio-frequency guidance, and fully autonomous navigation systems.

Fig. 3. Aboveground pipeline section

Underwater pipeline inspection vehicles (UPIVs) represent specialized craft equipped with 4K cameras, LED illumination systems, and sensor arrays capable of inspecting submerged infrastructure at depths ranging from 200 to 5,000 meters, thereby eliminating the need for hazardous diver operations. Prominent models such as the Chasing M2 Pro Max (Figure 4) incorporate sonar systems and manipulator arms for leak detection. This drone platform is engineered for complex subsea operations, inspections, and scientific research – enabling access to previously unreachable depths and facilitating investigations once deemed impracticable.

Fig. 4. Chasing M2 Pro Max underwater drone

Key advantages of the CHASING M2 PRO MAX include:

1. A 4K UHD camera with high light sensitivity produces detailed, vivid imagery even at significant depths and under low-light conditions, enabling precise image recognition for problem classification.

2. Modular architecture permits integration of supplementary equipment – including robotic manipulators, sonar systems, and specialized sensors – to address mission-specific requirements, affording exceptional operational flexibility.

3. Operational depth capability extending to 200 meters unlocks new possibilities for subsea research, permitting inspections and documentation in previously inaccessible locations.

4. Eight high-torque thrusters deliver superior maneuverability and stability in underwater currents, ensuring precise and reliable vehicle control under challenging hydrodynamic conditions.

5. Extended mission duration facilitated by swappable battery systems enables prolonged operations without frequent surfacing for recharging, thereby enhancing operational efficiency.

6. Intuitive mobile application interface with integrated intelligent functions simplifies operation even during complex mission profiles.

This industrial-grade underwater drone is designed for hydraulic structure inspection, vessel hull examination, drilling rig maintenance, pipeline and channel surveys, search and rescue operations, sediment and water sampling, and high-resolution video documentation. A coordinated system comprising multiple underwater drones and a drone port can rapidly and comprehensively inspect extended subsea pipeline segments, generating actionable intelligence for maintenance decision-making.

All data transmitted by the drone swarm accumulates within the drone port's information repository. Given the multiplicity of drones, redundant measurements of identical parameters for the same object may be transmitted concurrently. Furthermore, noise interference may corrupt transmitted signals. Consequently, prior to database storage, data must undergo denoising and consistency verification through a data fusion procedure integrating information from coherent sources (Hafeez et al., 2021, Smagin, 2012).

Following this filtering protocol, noise-reduced data – particularly slow trends – are archived within the monitoring information base. Data fusion redistributes the information flow, generating maxima and minima that more accurately reflect the monitored phenomenon. Integration of multi-source information enhances measurement precision and reliability beyond the capabilities of any single data source.

Sensor-acquired data undergo preliminary processing by the drone port's onboard processor to prevent heavily corrupted measurements from entering the operational database. Processed data are then accumulated in real time within the Blender 3D software suite's database to construct three-dimensional computer graphic models (Smagin, 2012).

Effective noise filtering reduces measurement uncertainty and enhances sensor accuracy. This process must address two noise categories: persistent noise (additive white Gaussian noise) with relatively stable amplitude, and random impulse interference induced by external factors.

Upon monitoring completion, all acquired information must be synthesized to generate a unified visual model representing both external and internal pipeline conditions (Marshal'ko et al., 2023). For maintenance and repair planning, visualization through graphical and video modeling provides an effective decision-support tool. Blender 3D software offers a convenient platform for constructing such models, enabling generation of visual representations of pipeline external and internal structure based on filtered data.

To prevent accidents and enhance pipeline operational safety and efficiency, autonomous monitoring systems incorporating artificial intelligence (AI) have been developed and deployed over recent (Islamov, et al., 2017; Askarov et al., 2018; Askarov et al., 2019; Tagirov et al., 2017; Iqbal et al., 2021; 2022; Erdelj et al., 2017).

Contemporary integrated monitoring systems typically incorporate machine intelligence software-neural networks – whose predictive accuracy for identifying failure-prone locations averages 95 %, substantially exceeding conventional defect detection methodologies.

AI-enabled software undergoes training using predefined parameters against databases containing extensive examples of adverse events and their consequences. This process enables the system to recognize correlations between input variables and expected outcomes, subsequently generating predictive models to identify or anticipate potential failures before they escalate into critical incidents (McDonald, 2019). For instance, the system may accurately detect equipment wear signatures or damage indicators and recommend appropriate remedial actions.

The AI system receives real-time pipeline condition data from the central data aggregation hub – the drone port – which collects signals from pipeline monitoring points and observer drone swarms. Artificial intelligence processes and interprets these inputs to generate assessments of current network status (Akay, 2022).

4. Conclusion

The monitoring methodology proposed in this article – employing drone ports and drone swarms for data acquisition, noise reduction, and fusion of coherent data sources – enhances the efficiency of pipeline maintenance planning and execution.

Implementation of automated year-round monitoring systems will enable condition-based pipeline operation, thereby reducing operational expenditures while ensuring operational safety.

References

Akay, 2022 – *Akay, S.S., Özcan, O., Şanlı, F.B.* (2022). Quantification and visualization of flood-induced morphological changes in meander structures by UAV-based monitoring. *Eng. Sci. Technol. Int. J.* 27. 101016.

Askarov et al., 2018 – *Askarov, R.M., Chuchkalov, M.V., Islamov, I.M., Tagirov, M.B., Kukushkin, A.N.* (2018). Specific features of longitudinal stress calculation for trunk gas pipelines based on in-line inspection data. *Oil Product and Hydrocarbon Transport and Storage*. 3: 37-44.

Askarov et al., 2019 – *Askarov, R.M., Kitaev, S.V., Islamov, I.M.* (2019). Technology for identifying pipeline sections with bending stresses at geodynamic zone crossings. *Bulletin of Tomsk Polytechnic University. Geo Assets Engineering*. 330(5): 18-25.

Atdaeva et al., 2024 – *Atdaeva, G., Agabaev, Sh., Amanazarov, O., Shaturaev, D.* (2024). Energy: The significance of energy in contemporary society. *IN SITU*. 10: 31-33.

Erdelj et al., 2017 – *Erdelj, M.; Natalizio, E.; Chowdhury, K.R.; Akyildiz, I.F.* (2017). Help from the sky: Leveraging UAVs for disaster management. *IEEE Pervasive Comput*. 16: 24-32.

Faniadis, Amanatiadis, 2020 – *Faniadis, E., Amanatiadis, A.* (2020). Deep Learning Inference at the Edge for Mobile and Aerial Robotics. *Proceedings of the 2020 IEEE International Symposium on Safety, Security, and Rescue Robotics, Abu Dhabi, United Arab Emirates, 4–6 November 2020*. Pp. 334-340.

Hafeez et al., 2021 – *Hafeez, A., Tiwari, V., Verma, V.K., Ansari, A.S., Husain, M.A., Singh, S., Khan, A.N.* (2021). Crop Monitoring and Automatic Weed Detection using Drone. *Proceedings of the 2021 International Conference on Control, Automation, Power and Signal Processing (CAPS), Jabalpur, India, 10–12 December 2021*. Pp. 1-4.

Iqbal et al., 2021 – *Iqbal, U. Barthelemy, J., Li, W., Perez, P.* (2021). Automating visual blockage classification of culverts with deep learning. *Appl. Sci.* 11. 7561.

Iqbal et al., 2022 – *Iqbal, U., Bin Riaz, M.Z., Barthelemy, J., Perez, P.* (2022). Quantification of visual blockage at culverts using deep learning based computer vision models. *Urban Water J.* 1-13.

Islamov, et al., 2017 – *Islamov, R.R., Aginei, R.V., Isupova, E.V.* (2017). Analysis of methods and tools for monitoring stress conditions of underground trunk oil and gas pipelines operating in complex engineering-geological environments. *Oil Product and Hydrocarbon Transport and Storage*. 6: 31-40.

Marshal'ko et al., 2023 – *Marshal'ko, Yu.S., Kuznetsov, N.K., Yuraido, B.F., Fedyukovich, G.I., Kuznetsov, K.* (2023). Development of automated monitoring systems for petroleum refining operations. *Modern Technologies. System Analysis. Modeling*. 1(77): 125-129.

McDonald, 2019 – *McDonald, W.* (2019). Drones in urban stormwater management: A review and future perspectives. *Urban Water J.* 16: 505-518.

Smagin, 2012 – *Smagin, S.A.* (2012). Application of the "Caterpillar" method for extracting quasi-deterministic jitter components in communication channels. Proceedings of Higher Educational Institutions. Volga Region. *Technical Sciences*. 1(21): 37-46.

Tagirov et al., 2017 – *Tagirov, M.B., Mustafin, F.M., Askarov, R.M., Bakiev, T.A.* (2017). Investigation of stress-strain state of a potentially hazardous trunk gas pipeline section. *Oil Product and Hydrocarbon Transport and Storage.* 2: 9-14.

Zhang et al., 2021 – *Zhang, H., Sun, M., Li, Q., Liu, L., Liu, M., Ji, Y.* (2021) An empirical study of multi-scale object detection in high resolution UAV mages. *Neurocomputing.* 421: 173-182.

Published in the USA
Biogeosystem Technique
Issued since 2014.
E-ISSN: 2413-7316
2025. 12(2): 85-97

DOI: 10.13187/bgt.2025.2.85
https://bgt.cherkasgu.press

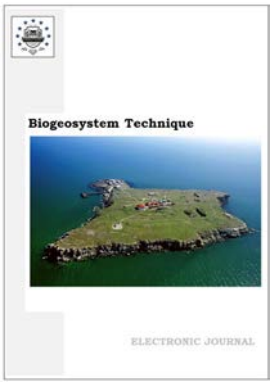

Effects of Light and Temperature on Photosynthetic Capacity of Mangrove Species in the Southern Coastal Region of Vietnam

Nguyen Van Thinh [a, *], Do Phong Luu [a], Ngo Trung Dung [b], Nguyen Trong Hiep [a], Mai Quang Tuyen [a], Dinh Vu Anh Tu [b], Alla A. Okolelova [c]

[a] Southern Branch of the Joint Vietnam-Russia Tropical Science and Technology Research Center, Ho Chi Minh, Vietnam
[b] Institute of Tropical Ecology, Joint Vietnam-Russia Tropical Science and Technology Research Center, Hanoi, Vietnam
[c] Volgograd State Technical University, Russian Federation

Paper Review Summary:
Received: 2025, October 2
Received in revised form: 2025, November 5
Acceptance: 2025, November 7

Abstract

Mangrove forests play a vital role in coastal protection and biodiversity maintenance, yet they are under severe pressure from climate change and human activities. This study evaluates the effects of light and temperature on the photosynthetic performance of five mangrove species (*Sonneratia alba*, *Avicennia alba*, *Excoecaria agallocha*, *Ceriops zippeliana*, and *Bruguiera gymnorrhiza*) in the southern coastal region of Vietnam, aiming to clarify their adaptability to climate change. We measured key photosynthetic parameters (A_{max}, light saturation point, and T_{opt}) at different canopy positions and analyzed their relationships with environmental variables. The results reveal significant differences in productivity and adaptation among species. *Avicennia alba* and *Ceriops zippeliana* exhibited higher photosynthetic capacity, while *Excoecaria agallocha* showed a higher light saturation point but lower productivity. The optimal temperature for photosynthesis ranged from 28–32 °C, with *E. agallocha* having a lower T_{opt}. These findings highlight the physiological diversity and adaptive traits of mangrove species that influence their distribution and ecological success under changing climates. The study provides scientific evidence for species selection in mangrove restoration and sustainable management strategies in the context of climate adaptation.

Keywords: mangrove plants, photosynthesis, climate change, light, temperature.

1. Introduction

Mangrove ecosystems play an exceptionally important role in environmental protection and the maintenance of biodiversity in coastal regions (Rahmadi et al., 2023), including in the southern areas of Vietnam (Dang et al., 2022). Mangrove forests not only provide habitats for numerous aquatic organisms and rare species of flora and fauna but also serve as a crucial natural barrier

* Corresponding author
E-mail addresses: thinh39b@gmail.com (N. Van Thinh)

protecting coastlines from erosion, mitigating the impacts of climate change, reducing wave energy, and preventing soil salinization (Nagelkerken et al., 2008; Rajpar, Zakaria, 2014). Moreover, these ecosystems offer significant economic and ecological benefits, such as fisheries resources, medicinal materials, and livelihoods for local communities (Bandaranayake, 1998; Hussain et al., 2010; Das et al., 2022). Therefore, the conservation and sustainable development of mangrove ecosystems have become an urgent task for scientists, environmental managers, and policy makers (Ferreira et al., 2022).

Photosynthetic capacity plays a central role in the growth and development of mangrove plants, reflecting not only their ability to capture solar energy but also their adaptability to harsh environmental conditions such as salinity, oxygen deficiency, and temperature fluctuations (Joshi et al., 1984; Nandy et al., 2007). In the context of intensifying climate change, studies on the photosynthetic performance of mangroves are crucial for assessing their adaptability and developing appropriate conservation strategies (Gilman et al., 2008; Ellison, 2015). Factors influencing photosynthesis include atmospheric composition, light intensity, salinity, temperature, and ecological competition (Sand-Jensen, 1989; Lovelock et al., 2016; Wang et al., 2021). In recent years, modern analytical technologies-such as automated photosynthesis systems, portable photosynthetic sensors, and Infrared Gas Analyzers (IRGA)-have enabled researchers to measure and monitor photosynthetic processes quickly and accurately, thereby identifying key influencing factors and proposing effective management solutions to enhance ecosystem resilience (Field et al., 1989; Tamayo et al., 2001; Douthe et al., 2018).

Automated photosynthesis systems, for instance those using Non-Dispersive Infrared (NDIR) technology to measure CO_2 and H_2O concentrations, allow for precise and continuous monitoring of leaf photosynthesis and transpiration under controlled conditions (Hodgkinson et al., 2013; Rolle et al., 2018). Portable photosynthesis sensors-such as chlorophyll fluorescence meters-provide a rapid and non-invasive method for evaluating photosynthetic performance and detecting early stress symptoms in plants (Dong et al., 2019; Herritt et al., 2020). Meanwhile, gas measurement instruments like the Infrared Gas Analyzer (IRGA) remain the standard tools for assessing leaf gas exchange rates and determining key physiological indicators such as A_{max}, CO_2 compensation point, and dark respiration (Toro et al., 2019; Macedo et al., 2021).

In the southern coastal region of Vietnam, mangrove ecosystems are increasingly affected by climate change, urbanization, industrialization, and excessive resource exploitation (Thanh et al., 2004; Giang et al., 2024). This region hosts many typical mangrove species such as *Avicennia marina*, *Rhizophora apiculata*, *Sonneratia alba*, and others that play essential roles in maintaining coastal ecological balance (Campbell, 2012; Warner et al. 2016; Do et al., 2022). However, physiological characteristics-especially photosynthetic capacity-of these species remain insufficiently investigated for conservation and sustainable management purposes. In fact, variations in photosynthetic performance can sensitively reflect negative environmental impacts (Krauss et al., 2008; Rovai et al., 2013), thereby helping to identify species most suitable for changing conditions or management interventions to enhance ecosystem resilience (Dasgupta et al., 2011).

Given the ecological importance of mangroves, studying the photosynthetic capacity of species in the southern coastal areas of Vietnam is essential to provide accurate and up-to-date physiological data under local environmental conditions. The main objectives of this paper are: (1) To evaluate the photosynthetic performance of several dominant mangrove species in southern Vietnam using modern analytical methods; and (2) To analyze environmental factors influencing their photosynthetic activity. The findings aim to provide a scientific foundation for practical applications in mangrove management, conservation, and sustainable development. This study not only supplies reliable physiological data but also enhances understanding of the ecological roles of mangrove species in coastal ecosystems, thereby supporting evidence-based conservation strategies and sustainable development initiatives.

2. Materials and methods

2.1. Study Species and Sites

The study was conducted on five mangrove species: *Sonneratia alba*, *Avicennia alba*, *Excoecaria agallocha*, *Ceriops zippeliana*, and *Bruguiera gymnorrhiza*. Representative individuals of each species were randomly selected from seven distinct study sites to ensure healthy and consistent growth conditions (Figure 1).

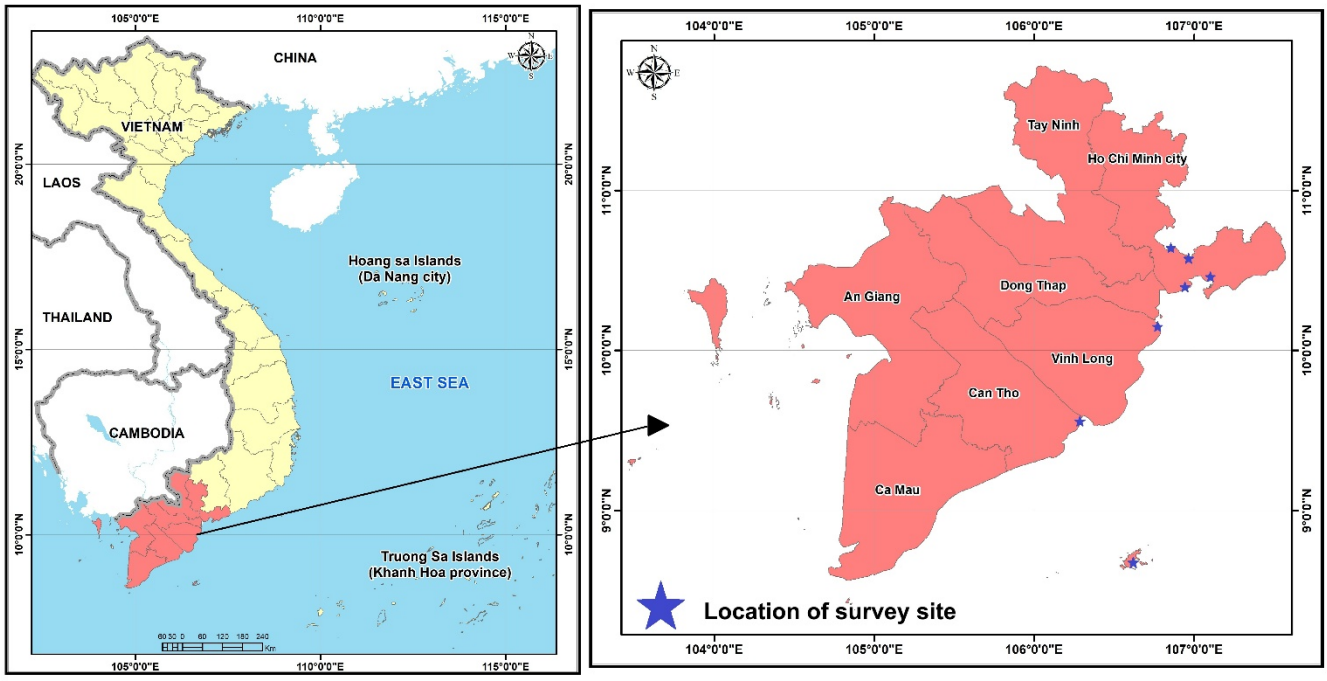

Fig. 1. Location map of the study sites

2.2. Sample Collection

To ensure representativeness and objectivity, the sampling process was carefully performed in accordance with standard scientific protocols (Figure 2). The selection of branches for measurement followed the criteria below:

Maturity: Selected branches carried fully mature leaves with a deep green color and stable size. Young, senescent, damaged, or diseased leaves were excluded.

Canopy position: To evaluate differences in photosynthetic activity at various canopy heights, samples were collected from three vertical positions: Upper, middle, and lower canopy. These positions were defined based on their relative height from the canopy apex and corresponding light availability.

Branch size: Each branch was cut to a length of 15–25 cm, ensuring a sufficient number of leaves for accurate measurement.

Sampling time: Collections were conducted in the early morning (8:00-10:00 a.m.), when photosynthetic activity was high and environmental conditions (temperature and humidity) were relatively stable.

Sample preservation: After cutting, branches were stored in polyethylene bags containing distilled water to maintain moisture and minimize dehydration. Samples were transported immediately to the laboratory and analyzed within two hours of collection.

Fig. 2. Field collection and photosynthesis measurement of mangrove plants at study sites

Adhering to these criteria ensured that the collected samples were representative of mangrove populations in the study area and that photosynthetic measurements were accurate and reliable.

2.3. Photosynthesis Measurement

Photosynthetic parameters were measured using the portable photosynthesis system LI-6800 (LI-COR Biosciences, Lincoln, Nebraska, USA) (LI-COR, 2023). The following environmental parameters were maintained within the measurement chamber: Leaf chamber air temperature: 30°C; Relative humidity: 70 %; CO_2 concentration: 400 µmol mol^{-1}. Each sample measurement was completed within five minutes, yielding approximately 20 recorded data points per run.

2.4. Data Analysis

Assuming that the intercellular CO_2 concentration in the mesophyll (Ci) is known from experimental data, the relationship between photosynthetic rate and light intensity was described using the biochemical model for C_3 photosynthesis proposed by Farquhar (Farquhar et al., 1980), commonly referred to as the *non-rectangular hyperbola model*: $\boldsymbol{\theta A_g^2 - A_g(a_i Q + A_{max}) J + a_i Q A_{max} = 0}$

Net photosynthetic rate (A_n) was calculated as: $\boldsymbol{A_n = A_g - R_d}$

Where: a_i is the initial quantum yield (mol mol^{-1}); A_n is the net photosynthetic rate; A_g is the gross photosynthetic rate; R_d is mitochondrial respiration (dark respiration); A_{max} is the maximum photosynthetic rate, and θ is the curvature factor of the light response curve, reflecting the degree of nonlinearity of the electron transport response. The model mainly involves the following parameters:

Initial quantum yield depends on C_i (µmol mol^{-1}), can be expressed by the Ball–Farquhar equation:

$$\boldsymbol{a_i = a_{io} \cdot (C_i - \Gamma) / (C_i + 2\Gamma)}$$

Where a_{io} is the maximum quantum yield of CO_2 assimilation and Γ (µmol mol^{-1}) is the CO_2 compensation point under non-photorespiratory conditions. The value of Γ increases with temperature due to the higher affinity of Rubisco for O_2 relative to CO_2. The relationship between Γ and leaf temperature (T_k, in Kelvin) is described as (Farquhar et al., 1989): $\boldsymbol{\Gamma = 1{,}7\, T_k}$

Intercellular CO_2 concentration (C_s): C_s varies with atmospheric CO_2 concentration (C_a); A_n and stomatal conductance (g_s). Under well-watered conditions, this relationship can be expressed using the semi-empirical Ball–Berry model (Ball et al., 1987):

$$\boldsymbol{g_s = \alpha \frac{A_n \cdot RH}{C_s} + g_o}$$

Where g_o is the residual conductance (experimentally determined), RH is relative humidity at the leaf surface, C_s is the CO_2 concentration at the leaf surface, and α is an empirical coefficient. Leuning later modified this model by substituting relative humidity (RH) with vapor pressure deficit (VPD) (Leuning, 1995):

$$\boldsymbol{g_s = \alpha \frac{A_n}{(C_i - \Gamma)(1 - VPD/VPD_o)} + g_o}$$

At low light (I → 0), $A_n \rightarrow 0$, and assuming $g_o \approx$ 0, we obtain:

$$\boldsymbol{C_i = C_s - \alpha (C_s - \Gamma)\left(1 + \frac{VPD}{VPD_o}\right)}$$

The maximum rate of photosynthesis A_{max} is primarily limited by Rubisco enzyme activity and depends on CO_2 concentration and temperature:

$$\boldsymbol{A_{max} = V_{max} \cdot (C_s - \Gamma)/(C_i + C)}$$

Where V_{max} is the maximum catalytic capacity of Rubisco per unit leaf area. The Michaelis constant (C) for CO_2 and O_2 in the Rubisco reaction is treated as constant in this study. The temperature dependence of V_{max} follows an Arrhenius-type relationship: $\boldsymbol{V_{max} = V_{m25}\{1 + exp[(-a_l + bT_a)/RT_a]\}^{-1}}$

Where: V_{m25} is the value at 25°C; a, b is the activation energy; R is the universal gas constant (8.314 J mol^{-1} K^{-1}), and T_a is absolute temperature (K).

3. Results and discussion

3.1. Dependence of Photosynthesis on Light Intensity and Temperature

The measured data on photosynthetic parameters of mangrove species in the southern coastal areas of Vietnam are presented in Table 1.

Table 1. Photosynthetic parameters of mangrove species in the southern coastal region of Vietnam

Species	Leaf position	A_{max} (µmol m^{-2} s^{-1})	Saturation PAR (µmol m^{-2} s^{-1})	Rd (µmol m^{-2} s^{-1})	Γ (µmol mol^{-1})	θ	A_{opt} (µmol m^{-2} s^{-1})	T_{opt} (°C)
Sonneratia alba	Upper canopy	6.2 ± 0.8	373 ± 13	-1.6 ± 0.2	15 ± 3	0.023	13.2 ± 0.4	31.7 ± 0.3
	Middle canopy	4.9 ± 0.7	358 ± 11	-1.1 ± 0.2	17 ± 3	0.022	13.0 ± 0.3	31.7 ± 0.2
	Lower canopy	3.8 ± 0.6	346 ± 12	-0.9 ± 0.2	16 ± 3	0.023	10.1 ± 0.3	30.5 ± 0.2
Avicennia alba	Upper canopy	10.2 ± 0.5	565 ± 17	-0.9 ± 0.2	12 ± 3	0.016	8.5 ± 0.5	29.3 ± 0.3
	Middle canopy	8.5 ± 0.4	562 ± 13	-0.9 ± 0.2	11 ± 3	0.016	11.1 ± 0.3	31.1 ± 0.2
	Lower canopy	7.7 ± 0.5	558 ± 9	-1.0 ± 0.2	12 ± 3	0.016	9.2 ± 0.3	28.7 ± 0.2
Excoecaria agallocha	Upper canopy	3.4 ± 0.3	1031 ± 11	-0.7 ± 0.2	34 ± 3	0.32	7.9 ± 0.4	26.5 ± 0.4
	Middle canopy	4.1 ± 0.3	1029 ± 18	-0.7 ± 0.2	31 ± 5	0.21	7.5 ± 0.4	30.1 ± 0.3
	Lower canopy	4.0 ± 0.3	1003 ± 28	-0.6 ± 0.2	32 ± 7	0.25	7.4 ± 0.4	24.7 ± 0.2
Ceriops zippeliana	Upper canopy	9.6 ± 0.4	531 ± 21	-0.7 ± 0.2	24 ± 5	0.02	14.3 ± 1.0	31.4 ± 0.4
	Middle canopy	10.1 ± 0.3	559 ± 28	-0.9 ± 0.3	18 ± 7	0.018	11.6 ± 0.7	29.8 ± 0.3
	Lower canopy	6.5 ± 0.3	527 ± 18	-1.7 ± 0.2	22 ± 4	0.021	10.3 ± 0.5	30.7 ± 0.2
Bruguiera gymnozhira	Upper canopy	8.2 ± 0.4	621 ± 13	-1.1 ± 0.2	21 ± 3	0.02	6.7 ± 0.3	28.8 ± 0.3
	Middle canopy	7.6 ± 0.3	613 ± 15	-0.8 ± 0.2	21 ± 3	0.02	6.3 ± 0.2	28.0 ± 0.2
	Lower canopy	7.5 ± 0.3	618 ± 20	-1.6 ± 0.2	21 ± 3	0.023	8.4 ± 0.2	28.2 ± 0.2

Analysis of the photosynthetic parameters of the five mangrove species (*Sonneratia alba*, *Avicennia alba*, *Excoecaria agallocha*, *Ceriops zippeliana*, and *Bruguiera gymnorrhiza*) revealed considerable variation in photosynthetic capacity, light saturation point, and optimal temperature among species and leaf positions (Table 1). This reflects physiological and adaptive differences of each species to distinct environmental conditions.

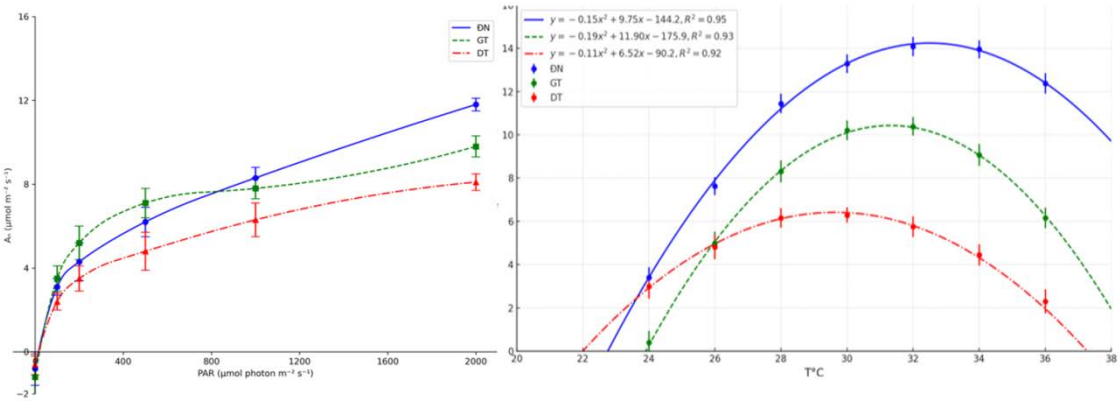

Fig. 3. Relationship between photosynthesis, light intensity, and temperature for *Sonneratia alba*.

The maximum photosynthetic rate (A_{max}), a key indicator of photosynthetic capacity, ranged from 3.4 ± 0.3 μmol m^{-2} s^{-1} (*Excoecaria agallocha*) to 10.2 ± 0.5 μmol m^{-2} s^{-1} (*Avicennia alba*). This indicates that *Avicennia alba* and *Ceriops zippeliana* tend to achieve higher photosynthetic performance than *Sonneratia alba*, *Bruguiera gymnorrhiza*, and especially *Excoecaria agallocha*. Variations in A_{max} values are often related to morphological and physiological traits such as leaf structure, chlorophyll content, and water-use efficiency.

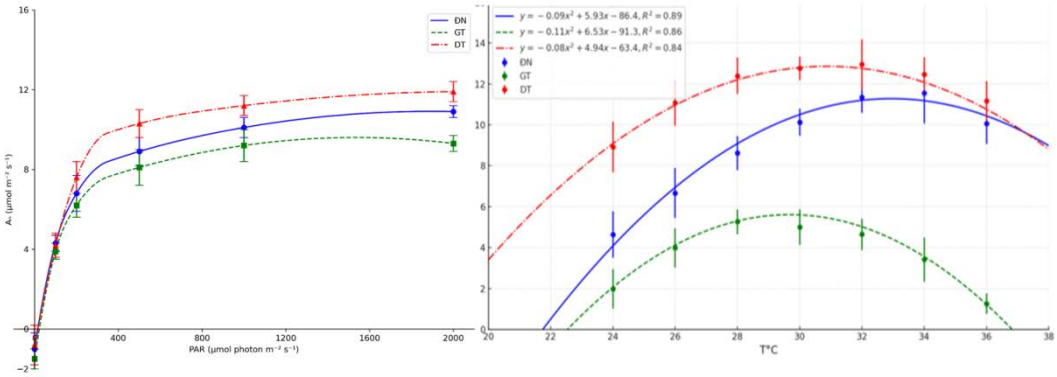

Fig. 4. Relationship between photosynthesis, light intensity, and temperature for *Avicennia alba*

The light saturation point, representing the light intensity required to achieve maximum photosynthesis, also varied among species. *Excoecaria agallocha* had the highest light saturation point (1003 ± 28 to 1031 ± 11 μmol m^{-2} s^{-1}), while the remaining species ranged between 346 ± 12 and 621 ± 13 μmol m^{-2} s^{-1}. This suggests that *E. agallocha* requires stronger light to reach optimal photosynthesis, whereas other species are better adapted to shaded or lower-light conditions.

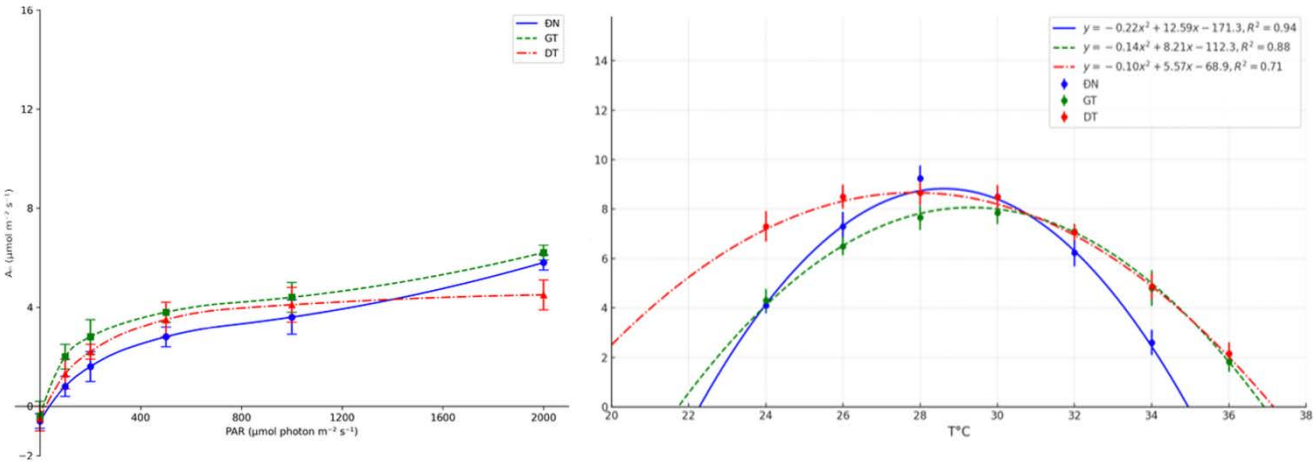

Fig. 5. Relationship between photosynthesis, light intensity, and temperature for *Excoecaria agallocha*

T_{opt} showed less variation among species compared to A_{max} or light saturation points. Most species exhibited T_{opt} values between 28°C and 32°C, consistent with tropical environmental conditions. *Excoecaria agallocha* showed slightly lower T_{opt} values (24.7 ± 0.2 to 30.1 ± 0.3°C), suggesting greater tolerance to cooler conditions.

Differences in photosynthetic capacity were also observed among canopy positions. Generally, A_{max} decreased from the upper canopy to the lower canopy, corresponding to light availability. However, the extent of this reduction varied among species, reflecting differing adaptation strategies.

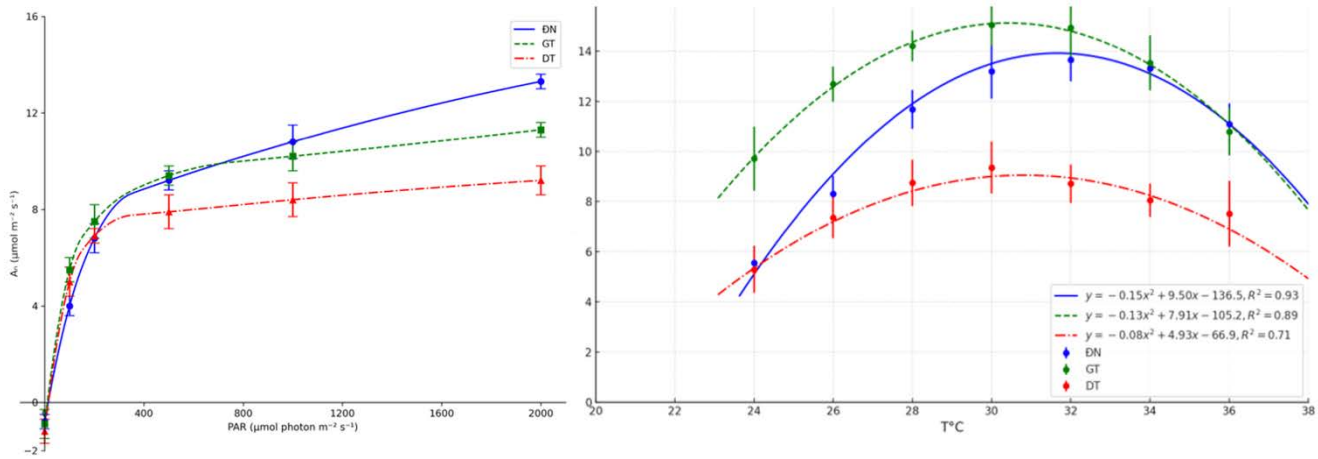

Fig. 6. Light and temperature dependence of photosynthesis in *Ceriops zippeliana*

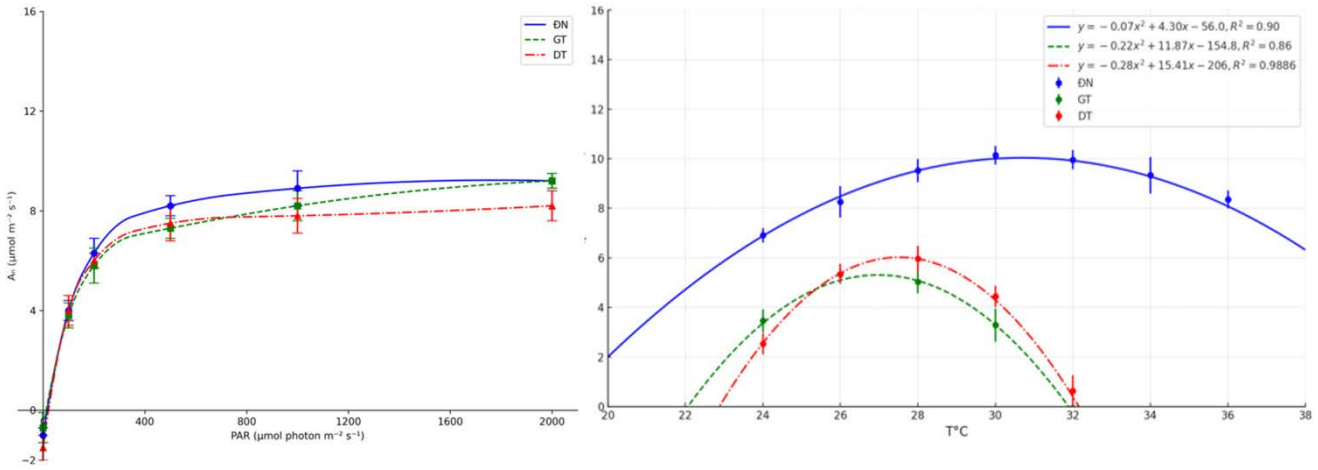

Fig. 7. Light and temperature dependence of photosynthesis in *Bruguiera gymnorrhiza*

According to Table 2, *Sonneratia alba* showed the greatest decrease in A_{max} (38.7 %), indicating significantly lower photosynthetic productivity in lower-canopy leaves. *Bruguiera gymnorrhiza* showed the smallest reduction (8.5 %), maintaining relatively high photosynthetic performance even under shade. Interestingly, *Excoecaria agallocha* showed a negative A_{max} reduction (-17.6 %), likely due to natural variability or increased exposure of lower leaves to diffused light.

Table 2. Variation of A_{max} by canopy position

Species	A_{max} (Upper canopy)	A_{max} (Lower canopy)	% Decrease
Sonneratia alba	6.2 ± 0.8	3.8 ± 0.6	38.7%
Avicennia alba	10.2 ± 0.5	7.7 ± 0.5	24.5%
Excoecaria agallocha	3.4 ± 0.3	4.0 ± 0.3	-17.6%
Ceriops zippeliana	9.6 ± 0.4	6.5 ± 0.3	32.3%
Bruguiera gymnorrhiza	8.2 ± 0.4	7.5 ± 0.3	8.5%

3.2. Comparison of Productivity and Adaptability among Mangrove Species

Photosynthetic Productivity

The maximum photosynthetic rate reflects the carbon fixation potential of plants. Results showed that *Avicennia alba* and *Ceriops zippeliana* achieved the highest A_{max} values (10.2 ± 0.5 and 9.6 ± 0.4 µmol m^{-2} s^{-1}, respectively, at upper canopy leaves), suggesting higher light-use

efficiency and growth potential under favorable conditions. Conversely, *Excoecaria agallocha* exhibited the lowest A_{max} (3.4 ± 0.3 μmol m^{-2} s^{-1}), indicating energy limitations under low light or strong competition.

A_{max} generally decreased from upper to lower canopy across most species, consistent with canopy light distribution. For instance, *Sonneratia alba* showed a pronounced reduction from 6.2 ± 0.8 to 3.8 ± 0.6 μmol m^{-2} s^{-1}, suggesting light limitation and reduced photosynthetic performance in shaded leaves.

Adaptation to Light Conditions

The light saturation point reflects a species' adaptation to light environments. *Excoecaria agallocha* exhibited the highest light saturation (>1000 μmol m^{-2} s^{-1}), indicating a requirement for high light intensity and confirming its pioneer role in open, disturbed, or newly accreted areas. In contrast, *Sonneratia alba* and *Bruguiera gymnorrhiza* had lower light saturation points, reflecting better adaptation to shaded or low-light environments such as beneath dense canopies. The curvature factor (θ) further supported these findings: light-demanding species showed lower θ values, indicating higher light-use efficiency.

Adaptation to Temperature

Table 3. Variation of T_{opt} by canopy position

Species	Upper canopy	Middle canopy	Lower canopy	Mean T_{opt}
Sonneratia alba	31.7 ± 0.3	31.7 ± 0.2	30.5 ± 0.2	31.3 ± 0.2
Avicennia alba	29.3 ± 0.3	31.1 ± 0.2	28.7 ± 0.2	29.7 ± 1.0
Excoecaria agallocha	26.5 ± 0.4	30.1 ± 0.3	24.7 ± 0.2	27.1 ± 2.3
Ceriops zippeliana	31.4 ± 0.4	29.8 ± 0.3	30.7 ± 0.2	30.6 ± 0.6
Bruguiera gymnorrhiza	28.8 ± 0.3	28.0 ± 0.2	28.2 ± 0.2	28.3 ± 0.4

In general, most species exhibited T_{opt} values within the range of 28–32°C, suitable for tropical environmental conditions. T_{opt} varied slightly among species (Table 3). *Sonneratia alba* showed the highest mean T_{opt} (31.3 ± 0.2°C), indicating superior tolerance to higher temperatures. *Excoecaria agallocha* exhibited the lowest mean T_{opt} (27.1 ± 2.3°C), suggesting better adaptation to cooler environments. Other species had intermediate T_{opt} values (28.3–30.6°C), consistent with tropical climatic conditions.

3.3. Adaptive Potential under Climate Change Scenarios

Based on the analysis of photosynthetic parameters, the adaptive responses of the five mangrove species were evaluated under climate change scenarios.

Sonneratia alba demonstrated strong adaptability to temperature increases under both RCP4.5 and RCP8.5 scenarios. Rising temperatures, if not accompanied by water scarcity, could enhance carbon assimilation and population growth in this species. *Avicennia alba* adapted well under RCP4.5 but showed reduced tolerance under RCP8.5, as extreme heat may exceed the optimal range for mid-canopy leaves, indicating vulnerability to heat stress.

Excoecaria agallocha was identified as sensitive to high solar radiation and unsuitable for areas with low rainfall and high annual sunshine. This species may struggle under hotter, drier climates. In contrast, *Ceriops zippeliana* exhibited strong light preference and adaptability to both RCP4.5 and RCP8.5 scenarios, showing flexible photosynthetic responses to increasing temperatures. *Bruguiera gymnorrhiza* also demonstrated resilience to thermal stress under both scenarios, with upper canopy leaves displaying superior resistance to heat and dehydration compared to lower leaves.

These results collectively highlight interspecific differences in photosynthetic capacity and resilience, offering critical insights for selecting and managing mangrove species in climate adaptation and restoration strategies.

3.4. Discussion

In the context of climate change and its increasing impacts on mangrove ecosystems, understanding the photosynthetic characteristics of individual species is of great importance-not

only to better comprehend their adaptive capacities but also to support smart and effective management decisions (Cheeseman et al., 1991; Cheeseman et al., 1997). The results of this study reveal notable differences in photosynthetic productivity and adaptability among five mangrove species. *Avicennia alba* and *Ceriops zippeliana* exhibited higher A_{max} values than the other species, whereas *Excoecaria agallocha* showed the highest light saturation point but the lowest A_{max}. T_{opt} among species ranged between 28-32°C, although *Excoecaria agallocha* tended to have lower T_{opt} values.

Differences in A_{max} may reflect variations in survival strategies and distribution patterns among mangrove species. *Avicennia alba* and *Ceriops zippeliana*, with higher A_{max} values, may be better adapted to nutrient-rich environments or possess a greater ability to compete for light. Conversely, *Excoecaria agallocha*, with its lower A_{max}, may be better suited to nutrient-poor or shaded environments (López-Hoffman et al., 2006; Wang et al., 2021). Such differences in A_{max} are often associated with variations in leaf morphology, chlorophyll content, water-use efficiency, and stomatal regulation capacity (Chang et al., 2022). The high light saturation point of *Excoecaria agallocha* aligns with its ecological role as a pioneer species typically found in open, high-light environments. In contrast, species with lower light saturation points-such as *Sonneratia alba* and *Bruguiera gymnorrhiza* – are better adapted to shaded conditions, for example, under dense canopy cover (Farnsworth et al., 1996; Ball, 2002; Krauss et al., 2003).

Differences in T_{opt} among species likely reflect adaptations to varying temperature regimes within the study region. The lower T_{opt} observed in *Excoecaria agallocha* suggests that this species may have originated from cooler habitats or possesses higher tolerance to lower temperatures (Field, 1995; Quisthoudt et al., 2012). Our results are consistent with previous studies on the photosynthetic responses of mangrove species (Moorthy et al., 1999; Das et al., 2002). However, some variations may result from differences in measurement methods, environmental conditions, or genetic characteristics among populations (Gutiérrez-Rodríguez et al., 2000; Reynolds et al., 2000).

Nevertheless, this study has several limitations that should be considered. First, measurements were conducted at a single time point (September 2023); thus, seasonal or environmental variations in photosynthetic performance could not be assessed (Suwa et al., 2008; Lele et al., 2021). Second, measurements were made only on mature leaves, so potential differences in photosynthetic response among developmental stages could not be evaluated (Okimoto et al., 2008). Furthermore, only five mangrove species were examined, preventing broad generalizations across all mangrove taxa in the region. Future studies should aim to measure photosynthetic parameters seasonally, across developmental stages, and under diverse environmental conditions to better understand temporal and physiological variations (Kaipiainen, 2009). Expanding research to include additional mangrove species will also provide a more comprehensive understanding of species diversity and functional adaptation in mangrove ecosystems.

The findings of this study have significant implications for understanding mangrove ecophysiology and for practical applications in mangrove restoration and management. Species selection for reforestation or rehabilitation projects can be guided by photosynthetic parameters such as A_{max}, light saturation point, and T_{opt}. Moreover, understanding how environmental factors affect mangrove photosynthesis can inform effective management strategies for protecting and restoring these critical ecosystems.

4. Conclusion

This study elucidated the differences in photosynthetic capacity among five key mangrove species in the southern coastal region of Vietnam, providing valuable insights into their ecology and adaptive mechanisms. The results demonstrate that *Avicennia alba* and *Ceriops zippeliana* possess higher photosynthetic productivity, while *Excoecaria agallocha* shows adaptation to high light intensity and lower temperature conditions. These findings highlight not only the physiological diversity among mangrove species but also offer essential scientific foundations for conservation and restoration efforts under changing climatic conditions. Selecting species that best match local environmental parameters is a crucial factor in ensuring the success of restoration projects.

For a more comprehensive understanding, future research should focus on assessing mangrove photosynthetic responses under varying environmental conditions (e.g., seasonal changes, salinity gradients, and pollution levels) and on examining genetic factors that may influence their adaptive

capacities. This study aims to contribute to raising awareness of the importance of mangrove conservation and to encourage concrete actions to protect these invaluable ecosystems for future generations.

5. Acknowledgments

This paper was completed based on data collected from the environmental protection project implemented during 2023-2024, led by the Southern Branch of the Joint Vietnam-Russia Tropical Science and Technology Research Center.

References

Ball et al., 1987 – *Ball, J.T., Woodrow, I.E., Berry, J.A.* (1987). A Model predicting stomatal conductance and its Contribution to the control of photosynthesis under different environmental conditions. Progress in Photosynthesis Research. Biggins, J. (eds.). Springer. Pp. 221-224.

Ball, 2002 – *Ball, M.C.* (2002). Interactive effects of salinity and irradiance on growth: implications for mangrove forest structure along salinity gradients. *Trees.* 16: 126-139. DOI: https://doi.org/10.1007/s00468-002-0169-3.

Bandaranayake, 1998 – *Bandaranayake, W.M.* (1998). Traditional and medicinal uses of mangroves. *Mangroves and Salt Marshes.* 2: 133-148. DOI: https://doi.org/10.1023/A:1009988607044

Campbell, 2012 – *Campbell, I.C.* (2012). Biodiversity of the Mekong Delta. In: The Mekong Delta System: Interdisciplinary Analyses of a River Delta. Renaud, F.G., Kuenzer, C. (eds.). Springer. Pp. 293-313.

Chang et al., 2022 – *Chang, Y., Fan, Y., Li, Z., Guanghui, L.* (2022). Relationship between photosynthetic characteristics, anatomical structure, and physiological indexes of two halophytes in different habitats. *Forests.* 13(12): 2189. DOI: https://doi.org/10.3390/f13122189.

Dang et al., 2022 – *Dang, N.T.An, Michael Reid, Lalit Kumar* (2022). Assessing potential impacts of sea level rise on mangrove ecosystems in the Mekong Delta, Vietnam. *Regional Environmental Change.* 22: 70. DOI: https://doi.org/10.1007/s10113-022-01925-z.

Das et al., 2002 – *Das, A., Parida, A., Basak, U., Das, P.* (2002). Studies on pigments, proteins and photosynthetic rates in some mangroves and mangrove associates from Bhitarkanika, Orissa. *Marine Biology*. 141:415-422. DOI: https://doi.org/10.1007/s00227-002-0847-0

Das et al., 2022 – *Das, S.C., Das, S., Tah,* J. (2022). Mangrove Forests and People's Livelihoods. In: Mangroves: Biodiversity, Livelihoods and Conservation. Das, S.C., Pullaiah, Ashton E.C. (eds.). Springer. Pp. 153-173.

Dasgupta et al., 2011 – *Dasgupta, N., Nandy, P., Das, S.* (2011). Photosynthesis and antioxidative enzyme activities in five Indian mangroves with respect to their adaptability. *Acta Physiologiae Plantarum*. 33: 803-810. DOI: https://doi.org/10.1007/s11738-010-0605-8

Do et al., 2022 – *Do, H.L., Dang, T.T.* (2022). Productivity response and production risk: A study of mangrove forest effects in aquaculture in the Mekong River Delta. *Ecological Economics.* 194: 107326. DOI: https://doi.org/10.1016/j.ecolecon.2021.107326

Dong et al., 2019 – *Dong, T., Shang, J., Chen, J.M., Liu, J., Qian, B., Ma, B., Morrison, M.J., Zhang, C., Liu, Y., Shi, Y., Pan, H., Zhou, G.* (2019). Assessment of portable chlorophyll meters for measuring crop leaf chlorophyll concentration. *Remote Sensing*. 11(22): 2706. DOI: https://doi.org/10.3390/rs11222706

Douthe et al., 2018 – *Douthe, C., Gago, J., Ribas-Carbó, M., Núñez, R., Pedrol, N., Flexas, J.* (2018). Measuring photosynthesis and respiration with infrared gas analysers. In: Advances in Plant Ecophysiology Techniques. Sánchez-Moreiras, A.M., Reigosa M.J., (eds.). Springer. Pp. 51-75.

Ellison, 2015 – *Ellison, J.C.* (2015). Vulnerability assessment of mangroves to climate change and sea-level rise impacts. *Wetlands Ecology and Management.* 23: 115-137. DOI: https://doi.org/10.1007/ s11273-014-9397-8

Farnsworth, Ellison, 1996 – *Farnsworth, E.J., Ellison, A.M.* (1996). Sun-shade adaptability of the red mangrove, Rhizophora mangle (Rhizophoraceae): Changes through ontogeny at several levels of biological organization. *American Journal of Botany*. 83(9): 1131-1143. DOI: https://doi.org/10.1002/j.1537-2197.1996.tb13893.x

Farquhar et al., 1980 – *Farquhar, G.D., Caemmerer, S., Berry, J.A.* (1980). A biochemical model of photosynthetic CO2 ssimilation in leaves of C3 species. *Planta*. 149: 78-90. DOI: https://doi.org/10.1007/BF00386231

Farquhar et al., 1989 – *Farquhar, G.D., Hubick, K.T., Condon, A.G., Richards, R.A.* (1989). Carbon Isotope Fractionation and Plant Water-Use Efficiency. In: Stable Isotopes in Ecological Research. Rundel, P.W., Ehleringer, J.R., Nagy, K.N. (eds.), Springer. Pp. 21-40.

Ferreira et al., 2022 – *Ferreira, A.C., Borges, R., Lacerda, L.D.* (2022). Can Sustainable Development Save Mangroves? *Sustainability*. 14(3): 1263. DOI: https://doi.org/10.3390/su14031263

Field et al., 1989 – *Field, C.B., Ball, J.T., Berry, J.A.* (1989). Photosynthesis: principles and field techniques. In: Plant Physiological Ecology: Field methods and instrumentation. Pearcy, R.W., Ehleringer, J.H., Mooney H.A., Rundel P.W. (eds.). Springer. Pp. 209-253.

Field, 1995 – *Field, C.D.* (1995). Impact of expected climate change on mangroves. In: Asia-Pacific Symposium on Mangrove Ecosystems. Wong, Y.S., Tam, N.F. (eds.). Springer. Pp. 75-81.

Giang et al., 2024 – *Giang, P.Q., Khanal, R.* (2024). What next for marine ecosystem management in Vietnam: assessment of coastal economy, climate change, and policy implication. *Environmental Research Communications.* 6:025002. DOI: https://doi.org/10.1088/2515-7620/ad19a5

Gilman et al., 2008 – *Gilman, E.L., Ellison, J., Duke, N.C., Field, C.* (2008). Threats to mangroves from climate change and adaptation options: A review. *Aquatic Botany*. 89(2): 237-250. DOI: https://doi.org/10.1016/j.aquabot.2007.12.009

Gutiérrez-Rodríguez et al., 2000 – Gutiérrez-Rodríguez, M., Reynolds, M.P., Larqué-Saavedra, A. (2000). Photosynthesis of wheat in a warm, irrigated environment: II. Traits associated with genetic gains in yield. Field Crops Research. 66(1):51-62. DOI: https://doi.org/10.1016/S0378-4290(99)00078-7.

Herritt et al., 2020 – *Herritt, M.T., Pauli, D., Mockler, T.C., Thompson, A.L.* (2020). Chlorophyll fluorescence imaging captures photochemical efficiency of grain sorghum (Sorghum bicolor) in a field setting. *Plant Methods.* 16: 109. DOI: https://doi.org/10.1186/s13007-020-00650-0

Hodgkinson et al., 2013 – *Hodgkinson, J., Smith, R., Ho, W.O., Saffell, J.R., Tatam, R.P.* (2013). Non-dispersive infra-red (NDIR) measurement of carbon dioxide at 4.2μm in a compact and optically efficient sensor. *Sensors and Actuators B: Chemical.* 186: 580-588. DOI: https://doi.org/10.1016/j.snb.2013.06.006

Hussain et al., 2010 – *Hussain, S.A., Badola, R.* (2010). Valuing mangrove benefits: contribution of mangrove forests to local livelihoods in Bhitarkanika Conservation Area, East Coast of India. *Wetlands Ecology and Management.* 18: 321-331. DOI: https://doi.org/10.1007/s11273-009-9173-3

Joshi et al., 1984 – *Joshi, G.V., Sontakke, S., Bhosale, L., Waghmode, A.P.* (1984). Photosynthesis and photorespiration in mangroves. In: Physiology and management of mangroves. Teas, H.J. (eds.). Springer. Pp. 1-14.

Kaipiainen, 2009 – *Kaipiainen, E.L.* (2009). Parameters of photosynthesis light curve in Salix dasyclados and their changes during the growth season. *Russian Journal of Plant Physiology*. 56: 445-453. DOI: https://doi.org/10.1134/S1021443709040025

Krauss et al., 2003 – *Krauss, K.W., Allen, J.A.* (2003). Influences of salinity and shade on seedling photosynthesis and growth of two mangrove species, Rhizophora mangle and Bruguiera sexangula, introduced to Hawaii. *Aquatic Botany*. 77(4): 311-324. DOI: https://doi.org/10.1016/j.aquabot. 2003.08.004

Krauss et al., 2008 – *Krauss, K.W., Lovelock, C.E., McKee, K.L., López-Hoffman, L., Ewe, S.M.L., Sousa, W.P.* (2008). Environmental drivers in mangrove establishment and early development: A review. *Aquatic Botany*. 89(2): 105-127. DOI: https://doi.org/10.1016/j.aquabot.2007.12.014

Lele et al., 2021 – *Lele, N., Kripa, M.K., Panda, M., Das, S.K., Nivas, A.H., Divakaran, N., Naik-Gaonkar, S., Sawant, A., Pattnaik, A.K., Samal, R.N., Thangaradjou, T., Saravanakumar, A., Rodrigues, B.F., Murthy, T.V.R.* (2021). Seasonal variation in photosynthetic rates and satellite-based GPP estimation over mangrove forest. Environmental Monitoring and Assessment. 193: 61. DOI: https://doi.org/10.1007/s10661-021-08846-0

Leuning, 1995 – *Leuning, R.* (1995). A critical appraisal of a combined stomatal-photosynthesis model for C3 plants. *Plant, Cell & Environment.* 18(4): 339-355. DOI: https://doi.org/10.1111/j.1365-3040.1995.tb00370.x

López-Hoffman et al., 2006 – *López-Hoffman, L., DeNoyer, J.N., Monroe, I.E., Shaftel, R., Anten, N.P., Martínez-Ramos, M., Ackerly, D.D.* (2006). Mangrove seedling net photosynthesis,

growth, and survivorship are interactively affected by salinity and light. *Biotropica*. 38(5): 606-616. DOI: https://doi.org/10.1111/j.1744-7429.2006.00189.x

Lovelock et al., 2016 – *Lovelock, C.E., Krauss, K.W., Osland, M.J., Reef, R., Ball, M.C.* (2016). The Physiology of Mangrove Trees with Changing Climate. In: Tropical Tree Physiology: Adaptations and Responses in a Changing Environment. Goldstein, G., Santiago L.S. (eds.). Springer. Pp. 149-179.

Macedo et al., 2021 – *Macedo, F.C., Daneluzzi, G.S., Capelin, D., Barbosa, F.S.,Silva, A.R., Oliveira, R.F.* (2021). Equipment and protocol for measurement of extracellular electrical signals, gas exchange and turgor pressure in plants. *MethodsX*. 8:101214. DOI: https://doi.org/10.1016/j.mex.2021.101214

Moorthy et al., 1999 – *Moorthy, P., Kathiresan, K.* (1999). Effects of UV-B radiation on photosynthetic reactions in Rhizophora apiculata. *Plant Growth Regulation*. 28: 49-54. DOI: https://doi.org/10.1023/A:1006279815159

Nagelkerken et al., 2008 – *Nagelkerken, I., Blaber, S.J.M., Bouillon, S., Green, P., Haywood, M., Kirton, L.G., Meynecke, J.O., Pawlik, J., Penrose, H.M., Sasekumar, A., Somerfield, P.J.* (2008). The habitat function of mangroves for terrestrial and marine fauna: A review. *Aquatic Botany*. 89(2): 155-185. DOI: https://doi.org/10.1016/j.aquabot.2007.12.007

Nandy et al., 2007 – *Nandy, P., Das, S., Ghose, M., Spooner-Hart, R.* (2007). Effects of salinity on photosynthesis, leaf anatomy, ion accumulation and photosynthetic nitrogen use efficiency in five Indian mangroves. *Wetlands Ecology and Management*. 15:347-357. DOI: https://doi.org/10.1007/s11273-007-9036-8.

Okimoto et al., 2008 – *Okimoto, Y., Nose, A., Ikeda, K., Agarie, S., Oshima, K., Tateda, Y., Ishii, T., Dang, N.D.* (2008). An estimation of CO2 fixation capacity in mangrove forest using two methods of CO2 gas exchange and growth curve analysis. *Wetlands Ecology and Management*. 16: 155-171. DOI: https://doi.org/10.1007/s11273-007-9062-6

Quisthoudt et al., 2012 – *Quisthoudt, K., Schmitz, N., Randin, C.F., Dahdouh-Guebas, F., Robert, E.M.R., Koedam, N.* (2012). Temperature variation among mangrove latitudinal range limits worldwide. *Trees*. 26: 1919-1931. DOI: https://doi.org/10.1007/s00468-012-0760-1

Rajpar, Zakaria, 2014 – *Rajpar, M.N., Zakaria, M.* (2014). Mangrove ecosystems of Asia: Status, challenges and management strategies. In: Mangrove Fauna of Asia. Faridah-Hanum, I., Latiff, A., Hakeem, K.R., Ozturk, M. (eds.). Springer. Pp. 153-197.

Rahmadi et al., 2023 – *Rahmadi, M.T., Yuniastuti, E., Suciani, A., Harefa, M.S., Persada, A.Y., Tuhono, E.* (2023). Threats to mangrove ecosystems and their impact on coastal biodiversity: A study on mangrove management in Langsa City. Indonesian Journal of Earth Sciences. 3(2):A627. DOI: https://doi.org/10.52562/injoes.2023.627.

Reynolds et al., 2000 – *Reynolds, M.P., Delgado, B.M.I., Gutiérrez-Rodríguez, M., Larqué-Saavedra, A.* (2000). Photosynthesis of wheat in a warm, irrigated environment: I: Genetic diversity and crop productivity. *Field Crops Research*. 66(1): 37-50. DOI: https://doi.org/10.1016/S0378-4290(99)00077-5

Rolle, Sega, 2018 – *Rolle, F., Sega, M.* (2018). Carbon dioxide determination in atmosphere by non dispersive infrared spectroscopy: A possible approach towards the comparability with seawater CO2 measurement results. *Measurement*. 128:479-484. DOI: https://doi.org/10.1016/j.measurement. 2018.07.007

Rovai et al., 2013 – *Rovai, A.S., Barufi, J.B., Pagliosa, P.R., Scherner, F., Torres, M.T.A., Horta, P.A., Simonassi, J.C., Quadros, D.P.C., Borges, D.L.D., Soriano-Sierra, E.J.* (2013). Photosynthetic performance of restored and natural mangroves under different environmental constraints. *Environmental Pollution*. 181: 233-241. DOI: https://doi.org/10.1016/j.envpol. 2013.06.023

Sand-Jensen, 1989 – *Sand-Jensen, K.* (1989). Environmental variables and their effect on photosynthesis of aquatic plant communities. *Aquatic Botany*. 34(1-3): 5-25. DOI: https://doi.org/10.1016/0304-3770(89)90048-X

Suwa, Hagihara, 2008 – *Suwa, R., Hagihara, A.* (2008). Seasonal changes in canopy photosynthesis and foliage respiration in a Rhizophora stylosa stand at the northern limit of its natural distribution. *Wetlands Ecology and Management*. 16: 313-321. DOI: https://doi.org/10.1007/s11273-007-9066-2

Tamayo et al., 2001 – *Tamayo, P.R., Weiss, O., Sánchez-Moreiras, A.M.* (2001). Gas exchange techniques in photosynthesis and respiration infrared gas analyser. In: Handbook of Plant Ecophysiology Techniques. Reigosa Roger, M. J. (eds.). Springer. Pp. 113-139.

Thanh et al., 2004 – *Thanh, T.D., Saito, Y., Huy, D.V., Nguyen, V.L., Ta, T.K.O., Tateishi, M.* (2004). Regimes of human and climate impacts on coastal changes in Vietnam. *Regional Environmental Change.* 4:49-62. DOI: https://doi.org/10.1007/s10113-003-0062-7

Toro et al., 2019 – *Toro, G., Flexas, J., Escalona, J.M.* (2019). Contrasting leaf porometer and infra-red gas analyser methodologies: an old paradigm about the stomatal conductance measurement. Theoretical and Experimental Plant Physiology. 31:483-492. DOI: https://doi.org/10.1007/s40626-019-00161-x

Wang et al., 2021 – *Wang, C.W., Wong, S.L., Liao, T.S., Weng, J.H., Chen, M.N., Huang, M.Y., Chen, C.I.* (2021). Photosynthesis in response to salinity and submergence in two Rhizophoraceae mangroves adapted to different tidal elevations. *Tree Physiology*. 42(5):1016-1028. DOI: https://doi.org/10.1093/treephys/tpab167

Wang et al., 2021 – *Wang, Y.S., Gu, D.J.* (2021). Ecological responses, adaptation and mechanisms of mangrove wetland ecosystem to global climate change and anthropogenic activities. *International Biodeterioration & Biodegradation.* 162: 105248. DOI: https://doi.org/10.1016/j.ibiod.2021.105248

Warner et al., 2016 – *Warner, R., Kaidonis, M., Dun, O., Rogers, K., Shi, Y., Nguyen, T.T.X., Woodroffe, C.D.* (2016). Opportunities and challenges for mangrove carbon sequestration in the Mekong River Delta in Vietnam. *Sustainability Science.* 11: 661-677. DOI: https://doi.org/10.1007/s11625-016-0359-3

Published in the USA
Biogeosystem Technique
Issued since 2014.
E-ISSN: 2413-7316
2025. 12(2): 98-103

DOI: 10.13187/bgt.2025.2.98
https://bgt.cherkasgu.press

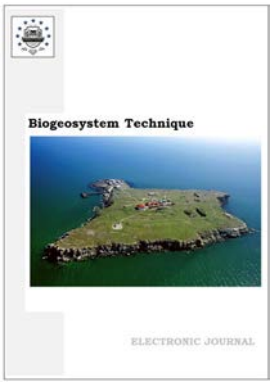

Short-Term Forecasting of Heavy Metal Concentrations in Soil: A Case Study of Some Regions of Armenia

Patrik Yesayan [a, *]

[a] National Polytechnic University of Armenia, Yerevan, Armenia

Paper Review Summary:
Received: 2025, November 12
Received in revised form: 2025, November 27
Acceptance: 2025, November 29

Abstract

The article examines the potential of forecasting methods to evaluate changes in the concentration of lithophilic chemical elements in soil samples, with a focus on scenarios in which limited monitoring data are available. The analysis is based on averaged chemical element concentrations, which enables assessment of the overall direction of change without reference to individual sampling points. This approach facilitates comparisons among elements, thereby allowing the identification of discrepancies in their temporal dynamics. The forecasts indicate that the concentrations of certain elements (Rb, Zr) remain unchanged, whereas those of others (Ba, Sr) show directional change or increased variability. It is imperative to account for this when interpreting pollution dynamics in the absence of detailed spatial data.

Keywords: heavy metals, artificial intelligence, machine learning, linear regression, exponential smoothing.

1. Introduction

The existing geochemical classification of chemical elements is based on their physicochemical properties, which are crucial to the formation of various geochemical systems (Perelman, 1989). However, the modern cycle of substances, exacerbated by anthropogenic environmental interventions, has become an irreversible geochemical factor in chemical migration. It is primarily due to the geochemical composition of the earth's surface. Actually, heavy metals are significant soil pollutants because they tend to accumulate and migrate through the soil over long periods (Gantulga et al., 2023; Sukiasyan et al., 2022). However, analyzing certain elements is difficult because they occur at trace and ultra-trace concentrations on the soil surface. Nonetheless, they form the foundation for the life and functioning of all biogeocenosis, from soils to living organisms. Lithophile elements stand out among these, mainly found in poorly soluble forms with low mobility and minimal participation in quick geochemical reactions (Isaev et al., 2025). Their behavior in soils mainly depends on the mineral makeup of parent rocks and overall geochemical conditions, rather than on local pollution sources. (Du Laing et al., 2009; Chougong et al., 2021).

* Corresponding author
E-mail addresses: patyesayan@gmail.com (P. Yesayan)

Consequently, it is essential to develop practical methods for controlling and monitoring environmental pollution, since data gaps often result from technical challenges in selecting and implementing geochemical techniques for these investigations (Sokolov et al., 2016).

In this context, employing artificial intelligence (AI) and machine learning (ML) models is crucial for real-time spatiotemporal environmental monitoring. This method addresses environmental challenges by handling diverse and often incomplete ecological data and integrating information on air, water, and soil quality assessments (Jordan et al., 2015; Xu et al., 2025). ML provides a more versatile and insightful analytical platform than traditional statistical methods, particularly for analyzing complex nonlinear relationships in geochemical systems (Shamsoddini, Esmaeil, 2023). ML also enables correction of anomalous values, identification of spatial trends, extraction of informative features, and improvement in the reliability of models for predicting the concentrations of chemical elements in natural environments (Ma et al., 2024; Alotaibi, Nassif, 2024).

One significant benefit of ML is its ability to automatically identify subtle data patterns and make predictions without requiring predefined functional dependencies, thereby enhancing the robustness of environmental modelling amid high uncertainty (Hao et al., 2023). Integrating ML methods into environmental research is especially crucial for evaluating soil pollution, as these datasets exhibit complex spatiotemporal patterns and are influenced by various natural and human-made factors (Gunal et al., 2023).

The article aims to address the practical challenge of enhancing environmental monitoring through AI and ML forecasting, particularly for assessing changes in soil chemical element concentrations when monitoring data are scarce.

2. Materials and methods

Soil samples were collected to a depth of 20 cm using the “envelope” method and non-metallic tools under dry-weather conditions. Target lithophile elements, including Zr, Sr, Rb, and Ba, were selected for analysis of soil from various regions in Armenia. Element concentrations were measured in the laboratory following standardized procedures (Sukiasyan, Kirakosyan, 2024). The sampling coordinates are listed in Table 1.

Table 1. Geographic coordinates of generalized sampling sites

Sampling sites		North	West
Hrazdan region	H1	40°33'04.9"	44°44'42.1"
	H2	40°33'10.4"	44°44'46.5"
	H3	40°33'29.2"	44°44'43.2"
Gavar region	G1	40°20'29.0"	45°12'22.6"
	G2	40°20'23.2"	45°12'16.8"
Martuni region	M1	40°13'49.8"	45°12'17.1"
	M2	40°13'48.5"	45°12'06.0"

The forecast model was built using data collected during a three-year monitoring period (2021–2023). These empirical data provided the foundation for modelling temporary fluctuations in concentrations. To ensure that forecasts of metal concentrations were physically realistic, a logarithmic transformation was applied before modelling. Specifically, the natural logarithm of the concentration values was computed as:

$$z_t = \log(y_t) \quad (1)$$

where y_t is the observed concentration at year t; z_t is the transformed value.

Two methods were used to model the temporal dynamics of Zr, Sr, Rb, and Ba concentrations: linear regression (LR) and exponential smoothing with a decaying trend (ETS) (Hyndman, Koehler, 2002; Koyande, 2024). LR was used to assess the trend direction (e.t, model the metal concentration as a linear function of time), and ETS was used to determine whether the trend was downward or stabilizing, extended to 2026:

$$\hat{z}_{t+k} = \beta_0 + \beta_1 x_{t+k} \quad (2)$$

where: $\hat{z}_{t+k}$ is the future values of concentration in log-space at year x_{t+k}; β_0 is the intercept; β_1 is the slope (rate of change over time).

The final predicted concentration can be calculated by:

$$\hat{y}_{t+k} = \exp(\hat{z}_{t+k}) \quad (3)$$

ETS is a state-space model. An additive error with an additive damped trend configuration is commonly applied for non-seasonal, short-term environmental data.

$$\hat{z}_{t+k} = l_{t-1} + \Phi b_{t-1} + \varepsilon_t \quad (4)$$

$$l_t = l_{t-1} + \Phi b_{t-1} + \alpha\varepsilon_t \quad (5)$$

$$b_t = \Phi b_{t-1} + \beta\varepsilon_t \quad (6)$$

where $\hat{z}_{t+k}$ is the future values of concentration in log-space at year x_{t+k}; ℓ_t is the level; b_t is the damped trend; ϕ is the damping parameter ($0 < \phi < 1$); α, β are smoothing parameters; ε_t is the forecast error.

The final predicted concentration can be calculated by:

$$\hat{y}_{t+k} = \exp(\hat{z}_{t+k}) \quad (7)$$

3. Results and discussion

Lithophile elements are the main sources of rock-forming minerals in Earth's crust (Lozovik et al., 2020). They exist as stable ions that form compounds with silicon and oxygen, such as silicates and oxides. These ions influence hydrolysis, oxidation-reduction, complexation, and precipitation in water, aiding the transfer of ions from water to soil (Alekin, Lyakhin, 1984). Soil samples collected annually from 2021 to 2023 were analyzed for Zr, Sr, Rb, and Ba. Table 2 shows the concentrations of these chemical elements in the grouped soil samples by year of collection.

Table 2. Concentration of the study lithophile element in soil sample

Sampling sites	Zr			Sr			Rb			Ba		
	2021	2022	2023	2021	2022	2023	2021	2022	2023	2021	2022	2023
H1	192.1	211.3	141.5	400.1	485.2	383.7	70.6	73.1	51.4	395.2	549.1	436.3
H2	335.3	228.2	211.0	468.2	396.5	359.8	77.7	63.9	53.6	477.4	447.2	570.7
H3	212.9	286.5	212.0	498.1	472.8	347.0	71.2	71.2	48.2	476.1	465.8	495.1
G1	186.7	184.3	147.0	527.4	565.0	515.3	60.8	57.7	41.6	436.3	537.8	578.9
G2	177.9	179.5	148.5	540.0	604.3	557.3	56.9	53.8	38.2	438.0	471.7	581.7
M1	173.3	179.4	132.1	381.1	408.5	341.7	73.4	68.8	50.2	284.3	393.4	382.3
M2	191.4	175.1	120.7	386.1	381.1	377.8	72.4	66.4	52.3	408.9	404.9	367.1

Then, to ensure reproducibility of the forecasting process, the numerical parameters of both predictive models (LR and ETS) are presented in Table 3.

Table 3. Comparison of parameters of both models: linear regression (LR) and exponential smoothing with a decaying trend (ETS)

Chemical element	LR model		ETS model				
	Intercept, β_0	Slope, β_1	Level	Trend	Damping	Initial Level	Initial Trend
Zr	286.41	-0.14	5.39	-0.14	0.995	209.94	-2.99
Sr	112.04	-0.05	6.16	-0.05	0.995	457.29	17.53
Rb	434.65	-0.21	4.29	-0.21	0.995	69.00	-3.00
Ba	-152.64	0.08	6.05	0.11	0.800	416.60	60.78

Figure 1 shows projected changes in soil concentrations of Zr, Sr, Rb, and Ba through 2026. Specifically, it presents a 95 % confidence interval for LR and a ±10 % uncertainty range for ETS.

Regarding Zr, the data up to 2023 show slight year-to-year variation, as seen in the simulation results. Subsequently, the LR model suggests a nearly flat trend through 2026, whereas the ETS model offers a smooth continuation of observed patterns with minor fluctuations. Throughout the forecast, the confidence intervals for both models remain narrow and only slightly

widen over time. Finally, the comparable widths of these intervals indicate low uncertainty and strong agreement between the models for Zr, consistent with its chemical inertia and incorporation into soil silicate phases.

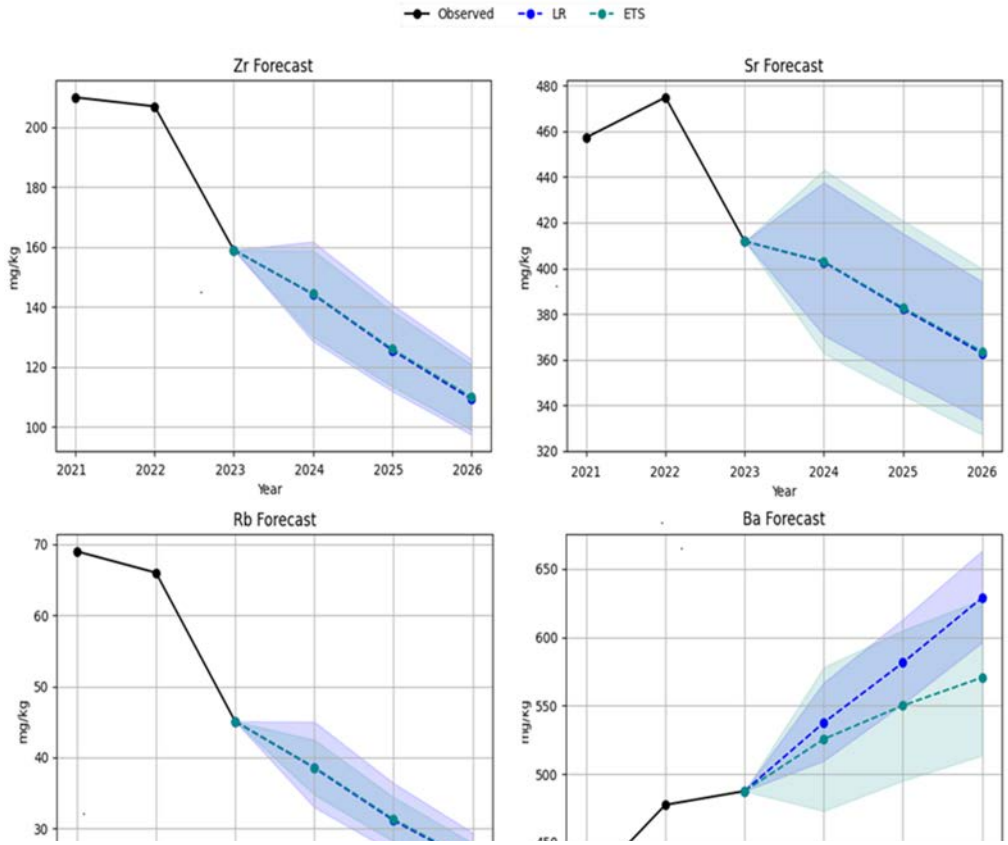

Fig. 1. Forecast of Zr, Sr, Rb, and Ba concentrations in soils through 2026 using linear regression (LR) and exponential smoothing with a decaying trend (ETS)

For Sr, LR suggests a weak directional trend that is consistently projected through 2026, indicating a modest expected change if current drivers persist. In contrast, ETS provides a smoother trajectory, signaling stability by actively preserving the present concentration level. The confidence intervals for both models gradually widen over the forecast period, a typical result of extrapolation, though they stay within observed value ranges. LR's slightly wider intervals compared to ETS's suggest this method is more responsive to year-to-year concentration variability, making it suitable for identifying shifts tied to short-term changes. This pattern reflects Sr's chemical behavior, such as its susceptibility to isomorphic calcium substitution and involvement in slow ion-exchange processes, meaning model outputs track the potential influence of these known mechanisms.

For Rb, the LR trend is very weak, with forecast values staying near the series' mean, suggesting no notable directional change under current conditions. The ETS model further flattens these dynamics, reinforcing an interpretation of long-term stability. Consistently narrow confidence intervals for both LR and ETS indicate little forecast uncertainty or expected change, which aligns with Rb's well-established fixation in potassium-rich soil minerals and amplifies confidence in status quo predictions.

For Ba, the predicted results also show high stability. LR produces a smooth, steady forecast. ETS smooths the dynamics, avoiding extremes. The confidence intervals for Ba widen only slightly and are similar across models. This shows moderate forecast uncertainty. The pattern reflects Ba's stable geochemical behavior, linked to carbonate and exchange forms. These results support using these predictions without accounting for regional differences. Building on this consistency, it is useful to examine how model behavior compares for short-term soil sample changes.

Short-term changes in soil sample concentrations were estimated using aggregated, non-spatial data. For Ba, both the LR and ETS models showed similar forecast directions and consistent trends. However, LR responded more to small, interannual fluctuations and produced more variable forecasts. ETS projections were more conservative, showing lower uncertainty over longer horizons. For lithophile elements, smoothing models like ETS are best, while LR supplements by gauging the overall trend.

4. Conclusion

Harnessing AI- and ML-based forecasting has unlocked new insights into spatiotemporal changes in lithophile element concentrations. When time-series data are limited, rely on ETS for a comprehensive assessment. For elements tightly bound to soil minerals and exhibiting low mobility, aggregated forecasting sharpens interpretation by highlighting stable background trends. Crucially, increasing model complexity or spatial detail yields only a slight improvement in forecast quality here. Ultimately, as our study affirms, align your model choice with both the data's statistical properties and the chemical characteristics of the elements.

References

Alekin, Lyakhin, 1984 – *Alekin, O.A., Lyakhin, Yu.I.* (1984). Ocean chemistry. Leningrad: Gidrometeoizdat, 344 p.

Alotaibi, Nassif, 2024 – *Alotaibi, E., Nassif, N.* (2024). Artificial intelligence in environmental monitoring: in-depth analysis. *Discover Artificial Intelligence*. 4: 84. DOI: https://doi.org/10.1007/s44163-024-00198-1

Chougong et al., 2021 – *Chougong D.T., Ngueutchoua G., Dicka E.H., Bessa, E.A.Z., Ghepdeu, Y.G.F., Bilounga, U.J.F., Yongue, F.R., Ntyam, S.C., Armstrong-Altrin, J.S.* (2021). Distributions of Trace Metals and Radionuclides Contamination in Alluvial Sediments from the Lobé River in Cameroon. *Earth Systems and Environment*. 6: 121-139. DOI: https://doi: 10.1007/s41748-021-00251-4

Du Laing et al., 2009 – *Du Laing, G., Rinklebe, J., Vandecasteele, B., Meers, E., Tack, F.M.G.* (2009). Trace metal behavior in estuarine and riverine floodplain soils and sediments: A review. *Science of the Total Environment*. 407(13): 3972-3985. DOI: https://doi:10.1016/j. scitotenv.2008. 07.025

Gantulga et al., 2023 – *Gantulga, N., Iimaa, T., Batmunkh, M., Surenjay, U., Tserennadmid, E., Turmunkh, T., Dechingungaa, D., Dorjsuren, B.* (2023). Impacts of natural and anthropogenic factors on soil erosion. *Proceedings of the Mongolian Academy of Sciences*. 63(2): 3-18. DOI: https://doi:10.5564/pmas.v63i02.1416

Gunal et al., 2023 – *Gunal, E., Budak, M., Kılıç, M., Cemek, B., Sırrı, M.* (2023). Combining spatial autocorrelation with artificial intelligence models to estimate spatial distribution and risks of heavy metal pollution in agricultural soils. *Environmental Monitoring and Assessment.* 195(2):317. DOI: https://doi:10.1007/s10661-022-10813-2

Hao et al., 2023 – *Hao, H., Li, P., Jiao, W., Ge, D., Hu, C., Li, J., Lv, Y., Chen, W.* (2023). Ensemble learning-based applied research on heavy metals prediction in a soil-rice system. *Science of The Total Environment*. 898:165456. DOI: https://doi:10.1016/j.scitotenv.2023.165456

Hyndman, Koehler, 2002 – *Hyndman, R., Koehler, A.* (2002). Forecasting with Exponential Smoothing: Some Guidelines for Model Selection. *International Journal of Forecasting*. 22(4): 443-473.

Isaev et al., 2025 – *Isaev, A.V., Sharafutdinov, R.N., Bogdanov, G.A.* (2025). Lithological and geochemical description of modern alluvial deposits in the middle reaches of the Bolshaya Kokshaga river. *Lomonosov geography journal*. 5:153-166. DOI: https://doi:10.55959/MSU0579-9414.5.80.5.12

Jordan, Mitchell, 2015 – *Jordan, M.I., Mitchell T.M.* (2015). Machine learning: Trends, perspectives, and prospects. *Science*. 349(6245): 255-260.

Koyande, 2024 – *Koyande T.* (2024). Assumption Checking of a Multiple Linear Regression Model. *International Journal of Research in Technology and Innovation*. 8(7): 322–325. [Electronic resource]. URL: http://www.ijrti.org/papers/IJRTI2407036.pdf

Lozovik et al., 2020 – *Lozovik, P.A., Kulik, N.V., Efremenko, N.A.* (2020). Lithophile elements and heavy metals in Lake Onega: sources, concentrations and transformation.

Transactions of the Karelian Scientific Centre of the Russian Academy of Sciences. 4: 62-74. DOI: https://doi:10.17076/lim1189

Ma et al., 2024 – *Ma, X., Guan, D., Zhang, C., Yu, T., Li, C., Wu, Z., Li, B., Geng, W., Wu, T., Yang, Z.* (2024). Improved mapping of heavy metals in agricultural soils using machine learning augmented with spatial regionalization indices. *Journal of Hazardous Mater*. 478:135407. DOI: https://doi: 10.1016/j.jhazmat.2024.135407

Perelman, 1989 – *Perelman, A.I.* (1989). Geochemistry. Moscow: Higher School.

Shamsoddini, Esmaeili, 2023 – *Shamsoddini, A., Esmaeili, S.* (2023). Modelling of soil heavy metal contamination using machine learning techniques and spectroscopic data. *The Journal of Spatial Planning and Geomatics*. 26(4): 139-160. [Electronic resource]. URL: http://hsmsp.modares.ac.ir/article-21-56457-en.html

Sokolov et al., 2016 – *Sokolov, S., Vlasov, N.G., Kurnik, L.P., Yurchenko, Yu.* (2016). The geochemical prospecting of the mineral deposits at the sites of the areal crust of weathering and the lacustrine-alluvial sediments increased power (by the example Pioneer-Pokrovsky ore cluster). *Exploration and protection of mineral resources*. 1. 15-21.

Sukiasyan et al., 2022 – *Sukiasyan, A., Simonyan, A., Kroyan, S., Hovhannisyan, A., Vardanyan, V., Okolelova, A., Kirakosyan, A.* (2022). Assessing the Geo-Environmental Risks of Technogenic Pollution of Agricultural Soils. *Biogeosystem Technique*. 9(2): 89-99. DOI: https://doi: 10.13187/bgt.2022.2.89

Sukiasyan, Kirakosyan, 2024 – *Sukiasyan, A.R., Kirakosyan, A.A.* (2024). Seasonal aspects of macro, trace, and ultra trace element changes in soils with different anthropogenic loads. *Sustainable Development of Mountain Territories*. 16(2): 789-802. DOI: https://doi.org/10.21177/1998-4502-2024-16-2-789-802

Xu et al., 2025 – *Xu, Y., Li, P., Zhang, Z., Gu, Y., Xiao, L., Liu, X., Wang, B.* (2025). Integrating machine learning for enhanced spatial prediction and risk assessment of soil heavy metal(loid)s. *Environmental Pollution*. 383. DOI: https://doi:10.1016/j.envpol.2025.126919